This manuscript is a preprint and has not been peer reviewed. The copyright holder has made the manuscript available under a Creative Commons Attribution 4.0 International (CC BY) license and consented to have it forwarded to EarthArXiv for public posting.

Contrasting Coal Power Trajectories in Southern Africa: Compound Air Pollution, Extreme Heat Exposure and the 2023 Hwange Expansion

Handsome Bongani Nyoni[1,*] Rutendo Mandeya[2], Daniel Tigere[3], Zororo Chinwadzimba[4], Rutendo Sibanda[4], Prosper Ncube[5], Perez Livias Moyo[5], Webster Gumindoga[6]

[1] Place Alert Labs, Department of Surveying and Geomatics, Faculty of the Built Environment, Midlands State University, Gweru, Zimbabwe

[2]Department of Electrical and Electronic Engineering, Faculty of Engineering and Built Environment, University of Zimbabwe

[3]Environmental Health Department, Shurugwi District Medical Office, Shurugwi, Zimbabwe

[4] Climate, Environment and Health Department, Centre for Sexual Health and HIV AIDS Research (CeSHHAR), Harare, Zimbabwe

[5]Department of Environmental Health, Faculty of Environmental Science, National University of Science and Technology, Bulawayo, Zimbabwe

[6]Department of Construction and Civil Engineering, Faculty of Engineering and Built Environment, University of Zimbabwe

* Corresponding authors: Handsome Bongani Nyoni (nyonih@staff.msu.ac.zw)

Short title: Compound pollution and heat risk around coal plants in Zimbabwe, Botswana and South Africa

This manuscript is a preprint and has not been peer reviewed. The copyright holder has made the manuscript available under a Creative Commons Attribution 4.0 International (CC BY) license and consented to have it forwarded to EarthArXiv for public posting.

1 Abstract

Coal-fired power generation is declining at many established sites in South Africa, while new capacity is being commissioned in drought-exposed parts of the Zambezi basin. This uneven transition raises concerns about the coincidence of industrial emissions, extreme heat and socioeconomic vulnerability. We assessed compound air-pollution and heat risk around coal power plants in Zimbabwe, Botswana and South Africa, focusing on atmospheric changes associated with the commissioning of Hwange Units 7 and 8 in Zimbabwe in 2023.

We screened 25 coal-fired power plants using open satellite, meteorological, population, and health-care accessibility datasets. Seventeen utility-scale plants had detectable nitrogen dioxide (NO_2) signals and were retained for comparative assessment. Hazard indicators comprised plant-associated excess tropospheric NO_2 and sulphur dioxide (SO_2) columns measured by TROPOMI, modelled fine particulate matter ($PM_{2.5}$), annual days exceeding 35 °C and land-surface heat anomalies. Exposure was characterised by residential populations within 25 km of each plant, while vulnerability was represented by young children, older adults and estimated travel time to health care. These measures were integrated into a compound risk index, with sensitivity analyses assessing rank stability. An interrupted time-series analysis and placebo-in-space comparison examined pollutant changes at Hwange following the commissioning of the additional generating units.

This manuscript is a preprint and has not been peer reviewed. The copyright holder has made the manuscript available under a Creative Commons Attribution 4.0 International (CC BY) license and consented to have it forwarded to EarthArXiv for public posting.

Pollution trajectories and overlapping climate-related hazards differed substantially among plants. At Hwange, post-commissioning NO_2 column excess increased by 9.4 µmol m^{-2} (95% confidence interval [CI]: 6.9–11.9), an 80% increase, while SO_2 excess increased by 63.0 µmol m^{-2} (95% CI: 37.6–88.4), or 103%. These were the largest increases among the 17 plants, contrasting with declining signals at most South African sites. Communities surrounding Hwange experienced approximately 57 days annually above 35 °C, compared with fewer than two days around plants on the South African Highveld. Hwange also exhibited a night-time land-surface heat excess of 2.3 °C and an estimated travel time to health care of 27 minutes, compared with 2–13 minutes near South African plants. Hwange ranked second among the 17 plants on the compound risk index, ranging from first to fourth in sensitivity analyses. Lethabo ranked highest, with approximately 722,000 residents within 25 km. Across all detectable plants, an estimated 1.86 million people, including 166,000 children under five, lived within 25 km. The pollution excess at Hwange peaked in 2024, coinciding with the greatest annual frequency of days above 35 °C in the analysed series.

This concurrence highlights potential compounding of air-pollution and heat hazards, but does not establish individual exposure, adverse health outcomes or causation by the newly commissioned units alone. Satellite column concentrations reflect atmospheric pollution signals rather than directly measured ground-level exposure; similarly, the compound index prioritises potential concern rather than estimating disease burden. By integrating multiple environmental hazards with population distribution and health-care accessibility, the approach provides a transparent,

This manuscript is a preprint and has not been peer reviewed. The copyright holder has made the manuscript available under a Creative Commons Attribution 4.0 International (CC BY) license and consented to have it forwarded to EarthArXiv for public posting.

reproducible screening framework to identify communities where new coal capacity intersects with climatic stress, supporting targeted monitoring, public-health preparedness and equitable energy-transition planning.

1.1 Author summary

New coal power units are being built in hot, drought-affected parts of southern Africa, often to make up for hydropower lost to drought. We used freely available satellite and population data to look at every coal plant in sub-Saharan Africa and asked where air pollution, extreme heat, many residents, and poor access to health care occur together. After two new units opened at Hwange in Zimbabwe in 2023, nitrogen dioxide around the plant rose by about four-fifths and sulphur dioxide doubled, the largest increases of any plant, while most South African plants declined. People in Hwange live with about two months a year above 35 °C and travel much further to reach a clinic than people near South African plants. When pollution, heat, population and access to care are considered together, Hwange ranks second in the region. Our open approach can help governments and communities see where new coal adds to climate stress on health.

This manuscript is a preprint and has not been peer reviewed. The copyright holder has made the manuscript available under a Creative Commons Attribution 4.0 International (CC BY) license and consented to have it forwarded to EarthArXiv for public posting.

2 Introduction

Air pollution is one of the leading environmental risks to health in Africa, and its burden is rising with industrial growth, energy demand and urbanisation. (Fisher et al., 2021). Coal-fired electricity is a concentrated source of nitrogen oxides, sulphur dioxide and primary particles, and it is also the most carbon-intensive way to generate power. Across sub-Saharan Africa, the coal fleet is dominated by South Africa, where most stations are ageing, and their output has fallen during years of breakdowns and load shedding. (Council for Scientific and Industrial Research, 2025). Elsewhere in the region, the trend runs the other way. New units have been built or planned in Zimbabwe, Zambia and Botswana, partly to secure supply when droughts reduce hydropower on the Zambezi (Conway et al., 2017; Global Energy Monitor, 2024). In late 2022, low water levels in Lake Kariba forced Zimbabwe to cap generation at the Kariba South station at 300 MW. (Al Jazeera, 2022), and the two new 300 MW units at Hwange Thermal Power Station were synchronised to the grid in March and June 2023 (Mining Index, 2023a, 2023b; Techzim, 2023).

These choices place additional pollution in places that are already among the hottest in southern Africa. Heat and air pollution act on the same cardiorespiratory pathways, and their joint effect on mortality can be larger than the sum of their separate effects.(Anenberg et al., 2020; Rai et al., 2023; Stafoggia et al., 2023) Africa is warming, heat exposure is increasing, and the capacity to adapt is uneven(Romanello et al., 2024). The exposome concept asks that such exposures be considered together, over the life course, rather than one pollutant at a time (Vermeulen et al., 2020; Wild, 2005).

This manuscript is a preprint and has not been peer reviewed. The copyright holder has made the manuscript available under a Creative Commons Attribution 4.0 International (CC BY) license and consented to have it forwarded to EarthArXiv for public posting.

The IPCC risk framework similarly treats risk as the product of hazard, exposure and vulnerability (IPCC, 2022). Applied to coal plants, this means asking not only how much a plant emits, but how many people live near it, how hot their environment is, and how well they can reach care.

Satellite observations make this possible where ground monitoring is sparse. The TROPOMI instrument on Sentinel-5P measures NO_2 and SO_2 columns daily at a resolution of a few kilometres (Theys et al., 2017; van Geffen et al., 2022; Veefkind et al., 2012)and its NO_2 retrievals resolve individual power plants and their changes in output (Beirle et al., 2019; Goldberg et al., 2019). In Zimbabwe, residents of Hwange have long raised concerns about dust and smoke from the power station and associated coal operations, but published measurements are scarce. (The Southern, 2024). No study has examined how the 2023 expansion changed pollution around Hwange, or how the risk around Hwange compares with the larger and better studied South African fleet.

We therefore asked three questions. First, which coal plants in sub-Saharan Africa produce a detectable pollution signal from space, and how did that signal change after mid 2023? Second, did the Hwange expansion increase NO_2 and SO_2 around the plant, and how does that change compare with other plants? Third, where do pollution, heat, population, and limited access to care coincide, and how does Hwange rank on a compound risk index? We used only open data so that the analysis can be repeated as new units come online.

This manuscript is a preprint and has not been peer reviewed. The copyright holder has made the manuscript available under a Creative Commons Attribution 4.0 International (CC BY) license and consented to have it forwarded to EarthArXiv for public posting.

3 Materials and methods

3.1 Study design and plants

This is an ecological, satellite-based exposure study with a quasi-experimental component. Plants were taken from the Global Power Plant Database version 1.3.0 (Global Energy Observatory et al., 2021), selecting those with coal as the primary fuel in sub-Saharan Africa (24 plants). Medupi in South Africa (4,764 MW), which the database omits, was added, giving 25 plants in South Africa, Zimbabwe, Zambia, Botswana, Namibia, Mauritius, Madagascar, and Niger (Fig. 1). National and provincial boundaries came from geoBoundaries gbOpen at a fixed release (commit 9469f09) (Runfola et al., 2020). A plant was treated as detectable when it had a capacity of at least 300 MW and a mean annual NO_2 excess (defined below) above 5 μmol m^{-2} with a t value above 3 across 2019 to 2025. Smaller plants were excluded because their signal could not be separated from that of the towns or industries around them. All processing used Google Earth Engine (Gorelick et al., 2017), Python 3.13 (Python Software Foundation, 2024) and statsmodels (R Core Team, 2024).

This manuscript is a preprint and has not been peer reviewed. The copyright holder has made the manuscript available under a Creative Commons Attribution 4.0 International (CC BY) license and consented to have it forwarded to EarthArXiv for public posting.

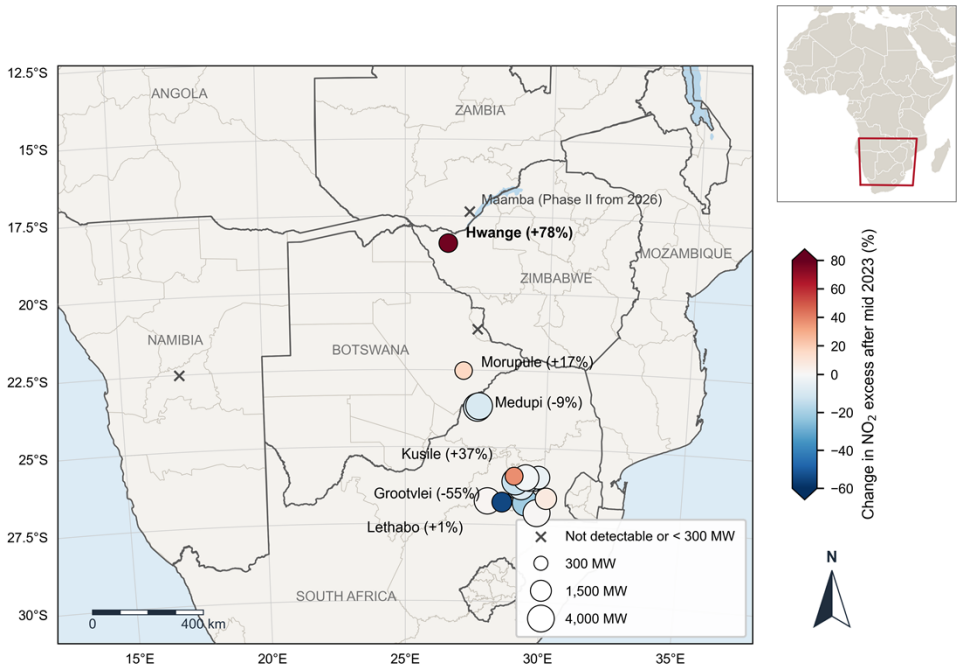


Fig 1. The shifting coal frontier in southern Africa. *Coal plants screened in this study, sized by capacity and coloured by the change in NO_2 excess between July 2018 and February 2023 and July 2023 and September 2026; crosses mark plants that were not detectable or smaller than 300 MW. Plants in Mauritius, Madagascar and Niger lie outside the map extent and had no detectable signal. Inset: location in Africa. Boundaries: geoBoundaries gbOpen ADM0 and ADM1; ocean, lakes and inset: Natural Earth. Lambert azimuthal equal-area projection.*

3.2 Pollution hazard

Tropospheric NO_2 columns and SO_2 columns came from the TROPOMI offline level 3 products in Earth Engine, which retain NO_2 pixels with a quality value above 0.75 (Theys et al., 2017; van Geffen et al., 2022; Veefkind et al., 2012). For each plant, we averaged columns within 10 km (the near zone) and within a background ring 40 to 80 km from the plant, excluding pixels within 15 km of any screened plant. The excess is the near-zone mean minus the background mean, in μmol m^{-2}. Subtracting a local background removes regional influences such as biomass burning, seasonal transport,

This manuscript is a preprint and has not been peer reviewed. The copyright holder has made the manuscript available under a Creative Commons Attribution 4.0 International (CC BY) license and consented to have it forwarded to EarthArXiv for public posting.

and changes in retrieval version that affect both zones alike (van Geffen et al., 2022). Annual means were computed for 2019 to 2025 for screening, and monthly means for July 2018 (NO_2) or December 2018 (SO_2) to September 2026 for the time series. Fire activity within 80 km of Hwange was summarised from FIRMS active fire detections to check whether burning could explain changes there. Fig. 2 maps the mean NO_2 column around every plant. For plant p and period t, the excess is

$$\Delta C_{p,t} = \overline{C}^{\mathrm{near}}_{p,t} - \overline{C}^{\mathrm{bg}}_{p,t} \quad (1)$$

where the bars denote mean columns in the near zone and in the background ring, a local-background contrast of the kind used to isolate point sources in satellite NO_2 (Beirle et al., 2019; Goldberg et al., 2019).

Annual $PM_{2.5}$ for 2017 to 2022 came from the 1 km Global High Air Pollutants (GHAP) product (Wei et al., 2023), the same product used in our earlier provincial assessment. (Nyoni et al., 2026). GHAP does not extend beyond 2022, so $PM_{2.5}$ describes the baseline burden around each plant and does not enter the before-and-after analysis. We report the population-weighted mean within 25 km and the near-zone excess over the background ring, defined as for NO_2.

This manuscript is a preprint and has not been peer reviewed. The copyright holder has made the manuscript available under a Creative Commons Attribution 4.0 International (CC BY) license and consented to have it forwarded to EarthArXiv for public posting.

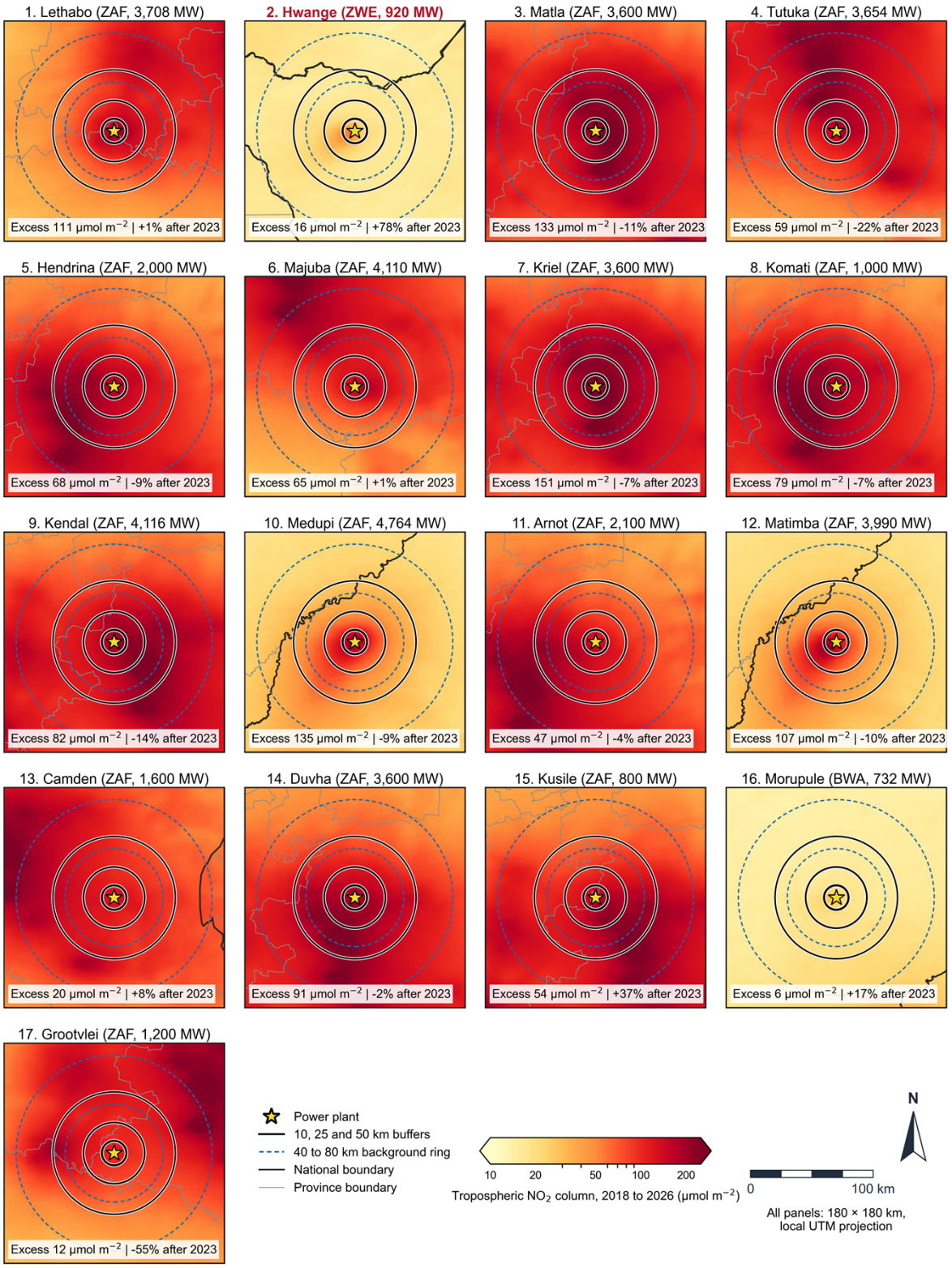


Fig 2. Tropospheric NO_2 around each detectable plant. *Mean TROPOMI tropospheric NO_2 column, July 2018 to September 2026 excluding the March to June 2023 transition, on one logarithmic scale for all plants. Labels give the mean annual NO_2 excess and its change after mid-2023. Panels are ordered by*

This manuscript is a preprint and has not been peer reviewed. The copyright holder has made the manuscript available under a Creative Commons Attribution 4.0 International (CC BY) license and consented to have it forwarded to EarthArXiv for public posting.

compound risk rank and share a 180 by 180 km extent in the local UTM projection, with the 10, 25 and 50 km buffers (black) and the 40 to 80 km background ring (blue dashed).

3.3 Heat hazard

Daily maximum 2 m air temperature came from ERA5-Land (Muñoz-Sabater et al., 2021). For each plant, we counted days above 35 °C per year, averaged over 2015 to 2024 and weighted by population within 25 km, and estimated the linear trend in annual mean daily maximum temperature from 1981 to 2024. Local surface heat was measured with MODIS Terra land surface temperature (MOD11A2, collection 6.1) (Wan, 2014) as the mean day-night difference between a 5 km zone around the plant and the background ring for 2019 to 2024. At Hwange, we also counted monthly hot days for 2018 to 2026 to examine whether pollution and heat coincided in time. Fig. 3 maps the night land surface temperature anomaly, each 1 km cell minus the mean of the plant's background ring.

This manuscript is a preprint and has not been peer reviewed. The copyright holder has made the manuscript available under a Creative Commons Attribution 4.0 International (CC BY) license and consented to have it forwarded to EarthArXiv for public posting.

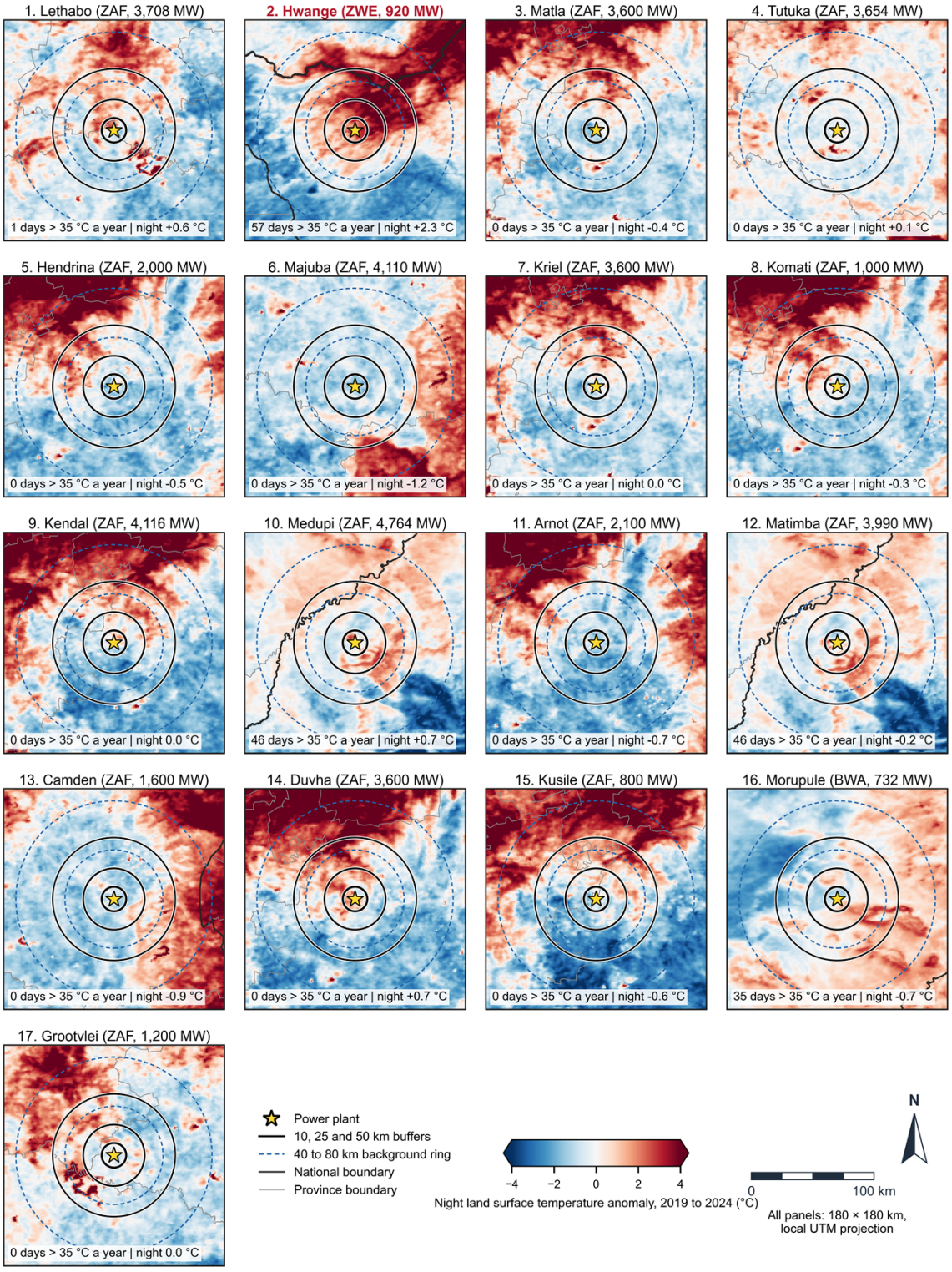


Fig 3. Night-time heat around each detectable plant. *Night land surface temperature anomaly, 2019 to 2024 (MODIS MOD11A2): each 1 km cell minus the mean of the plant background ring. Labels give the population-weighted number of days a year above 35 °C (ERA5-Land, 2015 to 2024) and the near-plant night excess.*

This manuscript is a preprint and has not been peer reviewed. The copyright holder has made the manuscript available under a Creative Commons Attribution 4.0 International (CC BY) license and consented to have it forwarded to EarthArXiv for public posting.

3.4 Exposure and vulnerability

Residential population, children under five and adults aged 65 and over came from the WorldPop 2020 unconstrained 100 m grids (WorldPop/GP/100m) (Tatem, 2017), summed within 10, 25 and 50 km of each plant. Totals across plants were computed from the union of buffers so that people living near more than one plant were counted once. Travel time to the nearest health facility came from the Malaria Atlas Project 2019 surface (Weiss et al., 2020), weighted by population within 25 km. Vulnerability combined the share of residents who are under five or 65 and over with this travel time. All zones were drawn in the local UTM projection of each plant so that buffers are true circles, and every plant was mapped at the same 180 by 180 km extent (Fig. 4). S1 Fig. gives one page per plant with the population surface, the change in NO_2 after mid-2023, and night land surface temperature. Population-weighted means of an indicator x over the cells i within a buffer were

$$\bar{x}_{\mathrm{pw}} = \frac{\sum_i P_i x_i}{\sum_i P_i} \tag{2}$$

where P_i is the population of cell i.

This manuscript is a preprint and has not been peer reviewed. The copyright holder has made the manuscript available under a Creative Commons Attribution 4.0 International (CC BY) license and consented to have it forwarded to EarthArXiv for public posting.

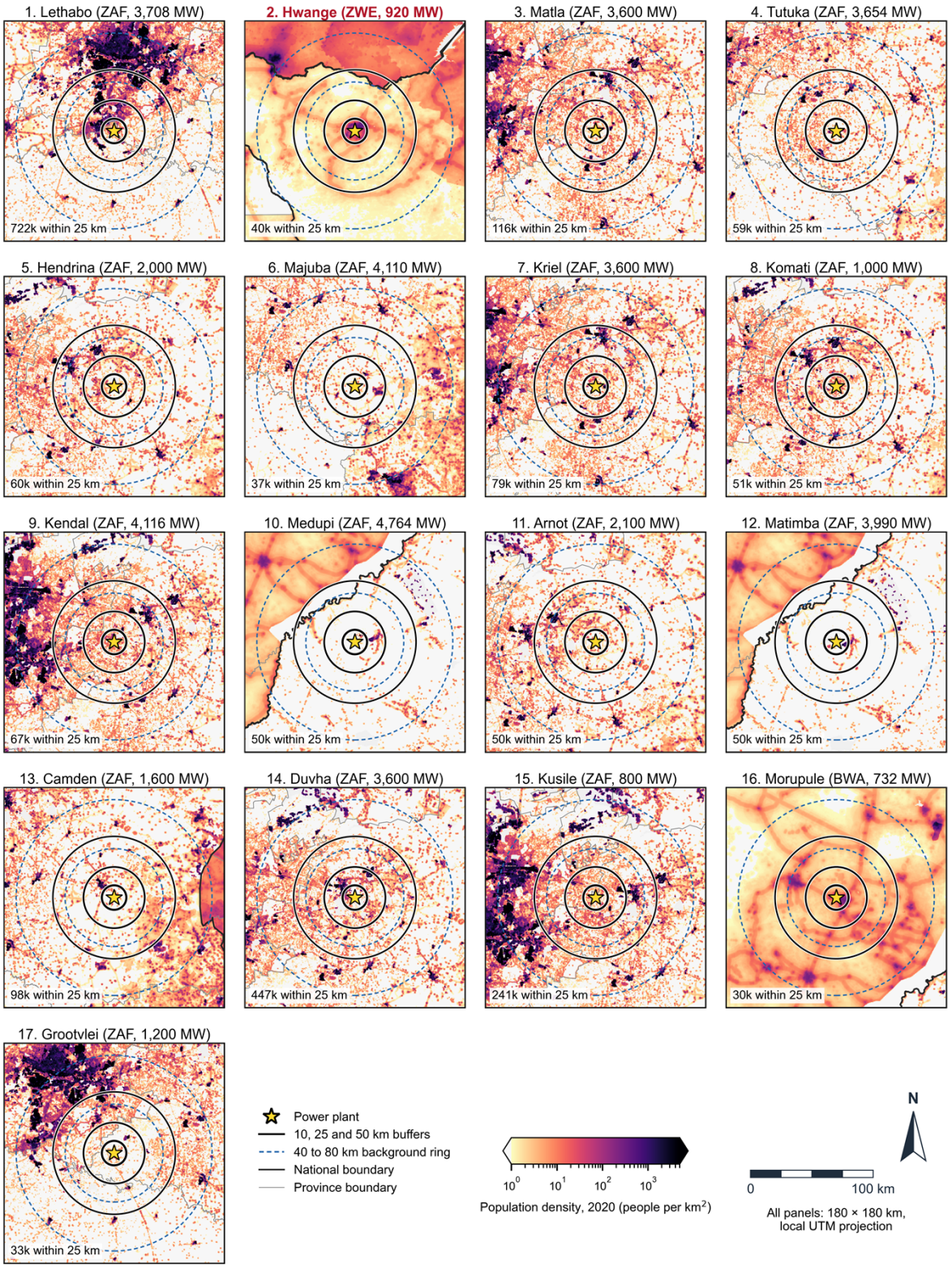


Fig 4. Population distribution and analysis zones around each detectable plant. *Population density (WorldPop 2020, 500 m cells) with the analysis zones; labels give the population within 25 km.*

This manuscript is a preprint and has not been peer reviewed. The copyright holder has made the manuscript available under a Creative Commons Attribution 4.0 International (CC BY) license and consented to have it forwarded to EarthArXiv for public posting.

3.5 Compound risk index

Following the IPCC framework (IPCC, 2022), each detectable plant received hazard, exposure, and vulnerability scores. Hazard was the mean of five indicators: NO_2 excess, SO_2 excess, $PM_{2.5}$ excess, population-weighted hot days, and night land surface heat excess. Exposure was the population within 25 km, and vulnerability was the mean of the two indicators above. Each indicator was scaled from 0 to 1 across the detectable plants (NO_2, SO_2 and population after log transformation), and the compound index was the geometric mean of the three domain scores, so that a plant ranks high only when all three domains are elevated. We assessed robustness by recomputing ranks with an arithmetic mean and by leaving out each hazard and vulnerability indicator in turn. Indicators were normalised as

$$x'_{k,p} = \frac{x_{k,p} - min_p x_{k,p}}{max_p x_{k,p} - min_p x_{k,p}} \quad (3)$$

and combined as

$$H_p = \frac{1}{n_H} \sum_{k \in H} x'_{k,p}, R_p = (H_p E_p V_p)^{1/3} \quad (4)$$

where E_p and V_p are formed in the same way from the exposure and vulnerability indicators. Min-max normalisation and geometric aggregation follow standard practice for composite indicators, in which a low score in one domain cannot be fully offset by a high score in another (IPCC, 2022; OECD & European Commission Joint Research Centre, 2008).

To show how compound risk is distributed around each plant, we also computed a cell-level index on the 1 km grid. For every populated cell (at least one person per km^2) within 50 km of the detectable plants, the mean NO_2 column, night land surface

This manuscript is a preprint and has not been peer reviewed. The copyright holder has made the manuscript available under a Creative Commons Attribution 4.0 International (CC BY) license and consented to have it forwarded to EarthArXiv for public posting.

249 temperature anomaly, population density and travel time to health care were converted
250 to percentile ranks q across all such cells, and

251 $$r_i = \left(\frac{q_i^{\mathrm{NO_2}} + q_i^{\mathrm{LST}}}{2} q_i^{\mathrm{pop}} q_i^{\mathrm{acc}}\right)^{1/3} \quad (5)$$

252 mirrors Eq. 4 at the scale of single cells. We report the number of people within 50 km
253 of each plant who live in cells in the top decile of r. Because hazard and vulnerability are
254 defined everywhere, we also mapped a continuous risk surface over every cell of each
255 window, replacing population density in Eq. 5 with the population within reach (density
256 smoothed with a Gaussian kernel, σ = 3 km) and pooling percentiles over all cells, and
257 summarised it as the population-weighted mean risk within 25 km. Both cell-level
258 surfaces are mapped in five classes split at the quintiles of all cells (very low to very
259 high), so that colours mean the same in every panel.

260 ### 3.6 Hwange expansion

261 The pre-expansion period was July 2018 to February 2023. Unit 7 was synchronised on
262 20 March 2023, and Unit 8 began supplying power around 9 June 2023 and reached full
263 output on 13 June (Mining Index, 2023a, 2023b; Techzim, 2023). March to June 2023
264 was treated as a transition, and July 2023 to September 2026 as the post-expansion
265 period. We fitted an interrupted time series to the monthly excess, with an indicator for
266 the post period and calendar-month fixed effects to remove seasonality, using Newey-
267 West standard errors with six lags (Lopez Bernal et al., 2017; Newey & West, 1987):

268 $$\Delta C_t = \alpha + \beta \mathrm{Post}_t + \sum_{m=2}^{12} \gamma_m M_{m,t} + \varepsilon_t \quad (6)$$

269 where $Post_t$ indicates the post-expansion months, $M_{m,t}$ the calendar-month indicators,
270 and β the change in excess. Sensitivity analyses added a linear time trend, counted the

This manuscript is a preprint and has not been peer reviewed. The copyright holder has made the manuscript available under a Creative Commons Attribution 4.0 International (CC BY) license and consented to have it forwarded to EarthArXiv for public posting.

transition months as post, and tested placebo break dates in July 2020, July 2021, and January 2022 within the pre period.

To compare Hwange with the rest of the fleet, we estimated a difference-in-differences across the 17 detectable plants, regressing the log ratio of near-zone to background NO_2 (and the SO_2 excess) on plant and month fixed effects and an indicator for the treated plant after July 2023:

$$\ln\left(\frac{C_{p,t}^{\text{near}}}{C_{p,t}^{\text{bg}}}\right) = \mu_p + \tau_t + \delta\left(D_p \times \text{Post}_t\right) + \varepsilon_{p,t} \quad (7)$$

Because only one plant was treated, inference used placebos in space (Abadie et al., 2010): each plant j was assigned the treatment in turn and

$$p = \frac{1}{N}\sum_{j=1}^{N} \mathbf{1}\left(\hat{\delta}_j \geq \hat{\delta}_{\text{Hwange}}\right) \quad (8)$$

So that with 17 plants the smallest attainable one-sided p-value is 0.059. We also report, for every plant, the change in mean excess between the same calendar months before and after July 2023.

3.7 Conditional health contrasts

Satellite columns are not ground-level concentrations, so we did not translate NO_2 or SO_2 into health effects. For $PM_{2.5}$ we estimated a conditional contrast for the near-zone excess, applying the long-term natural mortality risk ratio of 1.08 (95% CI 1.06 to 1.09) per 10 μg m^{-3} from the WHO systematic review (J. Chen & Hoek, 2020; World Health

This manuscript is a preprint and has not been peer reviewed. The copyright holder has made the manuscript available under a Creative Commons Attribution 4.0 International (CC BY) license and consented to have it forwarded to EarthArXiv for public posting.

Organization, 2021) to residents within 10 km, with national crude death rates averaged over 2017 to 2019 (World Bank, 2026):

$$AF_p = 1 - e^{-\beta \Delta \mathrm{PM}_{2.5,p}}, \beta = \frac{\ln \mathrm{RR}}{10}, D_p = AF_p \cdot \frac{\mathrm{CDR}_c}{1000} \cdot P_p \quad (9)$$

where $\Delta PM_{2.5,p}$ is the near-zone excess, CDR_c the crude death rate of country c, and P_p the population within 10 km. This contrast describes what the local $PM_{2.5}$ excess would imply if the published function applied; it is not an observed burden and is reported to show order of magnitude only.

3.8 Ethics and data availability

The study used only open, aggregated environmental and population data and involved no human participants, so ethics review was not required. All inputs are public, and the code and derived datasets are archived on Zenodo https://doi.org/10.5281/-zenodo.-23367004 as described in the data availability statement.

4 Results

4.1 Detectable plants and fleet-wide change

Of the 25 plants screened, 17 met the detection criteria: fifteen in South Africa, Hwange in Zimbabwe and Morupule in Botswana (Fig. 1, S1 Table). Plants in Mauritius, Madagascar and Niger showed little or no excess; Van Eck in Namibia was indistinguishable from the urban signal of Windhoek, and Maamba in Zambia (300 MW) had a mean NO_2 excess of only 1.7 μmol m^{-2}. Mean NO_2 excess ranged from 6.0 μmol m^{-2} at Morupule to 151.3 μmol m^{-2} at Kriel, and SO_2 excess was largest in the

This manuscript is a preprint and has not been peer reviewed. The copyright holder has made the manuscript available under a Creative Commons Attribution 4.0 International (CC BY) license and consented to have it forwarded to EarthArXiv for public posting.

Lephalale pair, Medupi (1,210 µmol m^{-2}) and Matimba (1,027 µmol m^{-2}). The NO_2 fields in Fig. 2 show compact plumes over the Lephalale pair and Hwange and a regional haze over the Highveld cluster.

After mid-2023, the NO_2 excess fell at most South African plants (Fig. 5), including declines of 22% at Tutuka and 55% at Grootvlei, and the SO_2 excess fell significantly at Medupi, Matimba, Kriel, Matla, Kendal and Tutuka. Kusile, a station still being completed during the study period, was the only South African plant with a clear NO_2 increase (+37%). Hwange showed the largest relative increases of any plant for both pollutants (+78% for NO_2 and +101% for SO_2 in the same calendar months)

.

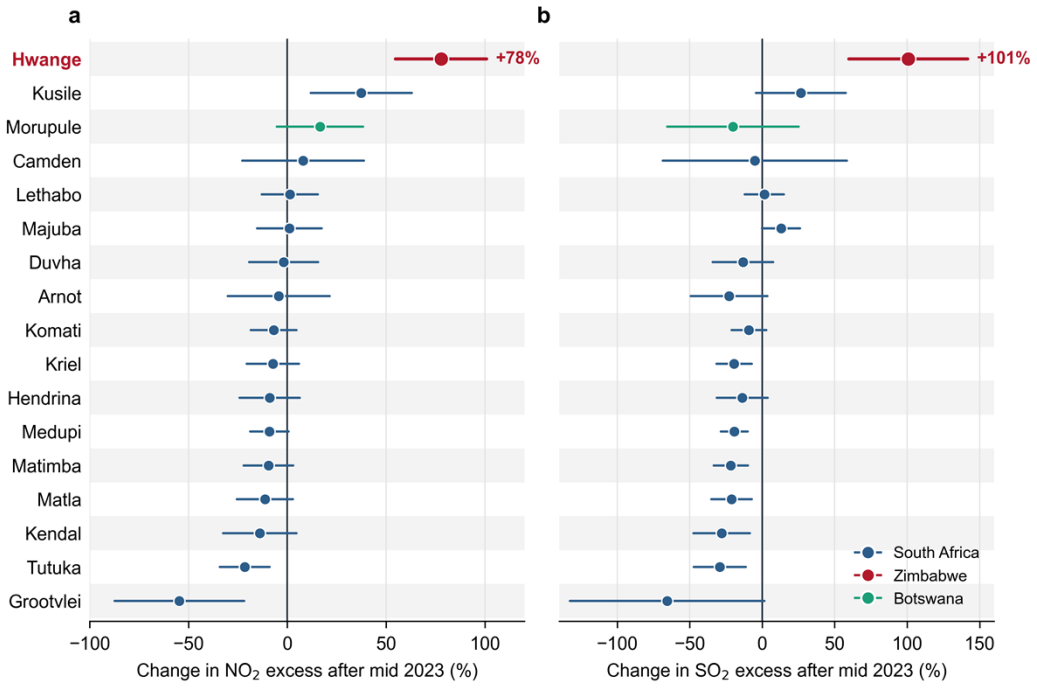


Fig 5. Change in pollution excess at each detectable plant after mid-2023. *Mean change between the same calendar months before (July 2018 to February 2023) and after (July 2023 to September 2026) as a percentage of the pre-period mean, with 95% confidence intervals. Hwange is shown in red*.

This manuscript is a preprint and has not been peer reviewed. The copyright holder has made the manuscript available under a Creative Commons Attribution 4.0 International (CC BY) license and consented to have it forwarded to EarthArXiv for public posting.

4.2 The Hwange expansion

Before the expansion, the NO_2 excess over Hwange averaged 11.8 μmol $m^{-2,}$ and the SO_2 excess 60.9 μmol m^{-2} (Fig. 6). Both rose through the transition and stayed higher thereafter. Adjusted for season, the NO_2 excess increased by 9.4 μmol m^{-2} (95% CI 6.9 to 11.9; 80%) and the SO_2 excess by 63.0 μmol m^{-2} (37.6 to 88.4; 103%) (Table 1). Estimates were larger with a linear trend (106% and 106%) and similar when the transition months were counted as post (75% and 96%). None of the placebo breaks within the pre-period produced an increase; the July 2020 break showed a decrease in NO_2, reflecting lower levels in 2020 to 2022 than in 2018 and 2019. In the difference-in-differences, Hwange had the largest estimate of the 17 plants for both NO_2 and SO_2 (placebo-in-space p = 0.059, the smallest attainable). Fire detections within 80 km did not track the change: 2024, the year with the highest NO_2 excess (22.9 μmol m^{-2}), had fewer fire detections within 80 km than every other full year except 2020.

The annual NO_2 excess was 10.3 μmol m^{-2} in 2020 to 2022 and 22.9 μmol m^{-2} in 2024. In the hottest months of the year, September to November, the NO_2 excess averaged 14.2 μmol m^{-2} before the expansion and 24.0 μmol m^{-2} in 2023 to 2025. The year 2024 had 94 days above 35 °C at Hwange, the most in the series, so the hottest period on record in these data coincided with the highest pollution excess (Fig. 6).

This manuscript is a preprint and has not been peer reviewed. The copyright holder has made the manuscript available under a Creative Commons Attribution 4.0 International (CC BY) license and consented to have it forwarded to EarthArXiv for public posting.

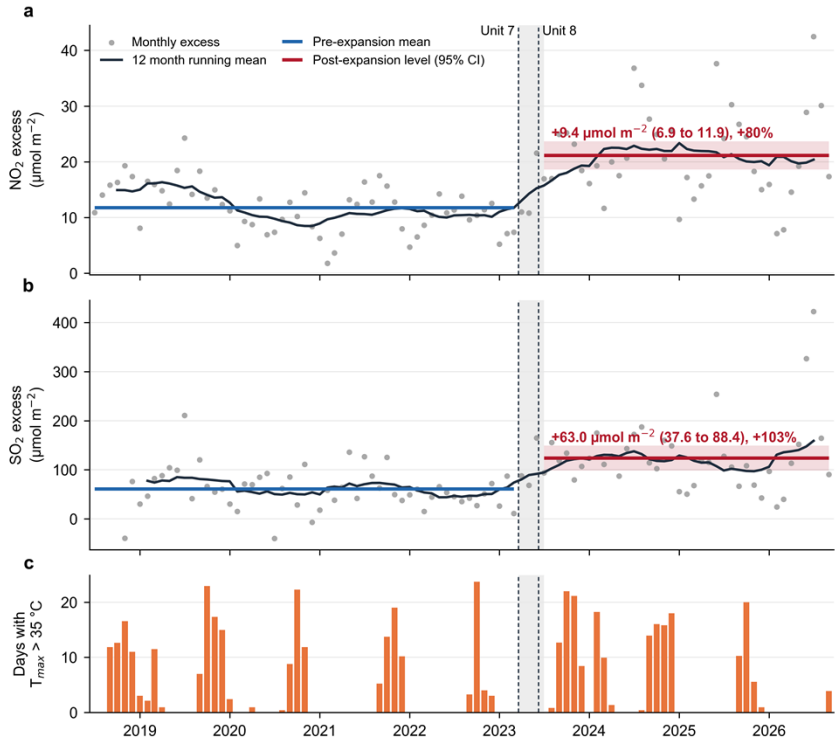


Fig 6. Pollution and heat at Hwange, July 2018 to September 2026. *Monthly NO_2 (a) and SO_2 (b) excess over the plant with 12-month running means; dotted lines show pre- and post-period means. Dashed lines mark the synchronisation of Unit 7 (20 March 2023) and Unit 8 (June 2023), and shading indicates the transition. (c) Days per month with maximum temperature above 35 °C (ERA5-Land).*

This manuscript is a preprint and has not been peer reviewed. The copyright holder has made the manuscript available under a Creative Commons Attribution 4.0 International (CC BY) license and consented to have it forwarded to EarthArXiv for public posting.

Table 1. Change in NO_2 and SO_2 excess over Hwange after the commissioning of Units 7 and 8.

Pollutant	Model	Months	Pre mean	Change (95% CI)	%	p
NO_2	Primary	95	11.8	9.4 (6.9 to 11.9)	80	<0.001
NO_2	With linear trend	95	11.8	12.5 (8.1 to 16.9)	106	<0.001
NO_2	Transition counted as post	99	11.8	8.8 (6.0 to 11.6)	75	<0.001
NO_2	Placebo break 2020-07	56	13.8	-3.7 (-5.9 to -1.5)	-27	0.001
NO_2	Placebo break 2021-07	56	12.2	-1.3 (-4.1 to 1.5)	-11	0.354
NO_2	Placebo break 2022-01	56	12.4	-1.8 (-4.3 to 0.6)	-15	0.149
SO_2	Primary	91	60.9	63.0 (37.6 to 88.4)	103	<0.001
SO_2	With linear trend	91	60.9	64.7 (21.5 to 107.9)	106	0.003
SO_2	Transition counted as post	95	60.9	58.4 (32.6 to 84.2)	96	<0.001
SO_2	Placebo break 2020-07	52	70.3	-16.3 (-37.9 to 5.2)	-23	0.138
SO_2	Placebo break 2021-07	52	62.6	-3.6 (-30.2 to 23.1)	-6	0.794
SO_2	Placebo break 2022-01	52	65.6	-15.6 (-35.9 to 4.7)	-24	0.132

Excess is the mean column within 10 km minus the mean in a 40 to 80 km background ring (μmol m^{-2}). Models include calendar-month fixed effects and Newey-West standard errors (6 lags). Pre: July 2018 to February 2023; post: July 2023 to September 2026; transition: March to June 2023. Placebo breaks use pre-period data only.

4.3 Heat, population and vulnerability

Heat exposure differed sharply across the fleet (Fig. 3, Table 2). Residents near Hwange experienced 57 days a year above 35 °C, compared with 46 near Medupi and Matimba, 35 near Morupule and fewer than two near every plant on the Highveld. Hwange also had the largest night-time land surface heat excess of any detectable plant (2.3 °C), with a daytime excess of 1.3 °C. The long-term warming trend in daily maximum temperature was weaker at Hwange (0.07 °C per decade, 1981 to 2024) than on the Highveld (0.38 to 0.50 °C per decade), so the heat hazard at Hwange reflects a hot climate rather than unusually fast local warming.

This manuscript is a preprint and has not been peer reviewed. The copyright holder has made the manuscript available under a Creative Commons Attribution 4.0 International (CC BY) license and consented to have it forwarded to EarthArXiv for public posting.

In total, 228,000 people live within 10 km, 1,860,000 within 25 km and 4,810,000 within 50 km of the 17 detectable plants, including 166,000 children under five and 90,000 adults aged 65 and over within 25 km. Lethabo, on the edge of the Vaal industrial area, had the largest population within 25 km (722,000; Fig. 4), followed by Duvha (447,000) and Kusile (241,000). Hwange had 39,800 residents within 25 km, most of them (32,900) within 10 km in the town itself. Travel time to health care near Hwange (27 minutes) was more than twice the longest near any South African plant (13 minutes).

Population-weighted $PM_{2.5}$ in 2017 to 2022 ranged from 12.6 μg m^{-3} near Hwange to 31.3 μg m^{-3} near Lethabo, above the WHO guideline of 5 μg m^{-3} everywhere (World Health Organization, 2021). The near-zone $PM_{2.5}$ excess was small at Hwange (0.4 μg m^{-3}) and up to 6.8 μg m^{-3} on the Highveld. Applied to residents within 10 km, the conditional mortality contrasts for this excess ranged from zero to 11 deaths a year per plant, with 0.9 at Hwange (S1 Table).

This manuscript is a preprint and has not been peer reviewed. The copyright holder has made the manuscript available under a Creative Commons Attribution 4.0 International (CC BY) license and consented to have it forwarded to EarthArXiv for public posting.

Table 2. Hazard, exposure, vulnerability and compound risk for the detectable utility-scale coal plants.

Plant	Country	MW	NO_2	SO_2	Hot days	LST night	Population	Travel	Index	Rank
Lethabo	ZAF	3,708	111.4	412	1	0.6	721,959	2	0.43	1 (1–10)
Hwange	ZWE	920	16.1	87	57	2.3	39,783	27	0.33	2 (1–4)
Matla	ZAF	3,600	132.6	552	0	-0.4	116,371	6	0.28	3 (2–11)
Tutuka	ZAF	3,654	58.8	220	0	0.1	59,431	4	0.27	4 (2–9)
Hendrina	ZAF	2,000	67.7	205	0	-0.5	60,111	10	0.26	5 (4–8)
Majuba	ZAF	4,110	65.5	342	0	-1.2	37,336	3	0.25	6 (3–14)
Kriel	ZAF	3,600	151.3	587	0	0.0	79,365	6	0.25	7 (3–16)
Komati	ZAF	1,000	79.1	237	0	-0.3	50,832	13	0.24	8 (5–17)
Kendal	ZAF	4,116	82.2	384	0	0.0	66,988	6	0.21	9 (6–13)
Medupi	ZAF	4,764	135.0	1,210	46	0.7	49,821	2	0.21	10 (6–13)
Arnot	ZAF	2,100	46.8	147	0	-0.7	49,743	8	0.21	11 (8–13)
Matimba	ZAF	3,990	107.2	1,027	46	-0.2	49,828	2	0.21	12 (7–14)
Camden	ZAF	1,600	19.9	59	0	-0.9	98,493	2	0.21	13 (5–16)
Duvha	ZAF	3,600	91.0	334	0	0.7	447,389	2	0.20	14 (7–14)
Kusile	ZAF	800	54.5	169	0	-0.6	240,504	2	0.14	15 (11–15)
Morupule	BWA	732	6.0	30	35	-0.7	30,233	12	0.11	16 (15–17)
Grootvlei	ZAF	1,200	12.5	34	0	0.0	33,269	4	0.11	17 (14–17)

NO_2 and SO_2: mean annual excess, 2019 to 2025 (μmol m^{-2}). Hot days: population-weighted days with maximum temperature above 35 °C within 25 km, 2015 to 2024. LST night: night land surface temperature excess, 2019 to 2024 (°C). Population: WorldPop 2020 within 25 km. Travel: population-weighted travel time to health care within 25 km (minutes). Index: geometric mean of hazard, exposure and vulnerability scores; rank range across leave-one-indicator-out analyses in brackets.

4.4 Compound risk

Lethabo ranked first on the compound index (0.43), driven by exposure, and Hwange second (0.33), driven by hazard and vulnerability (Table 2, S2 Fig.). Hwange combined the highest vulnerability score (0.74) with a hazard score (0.55) in the top third of the fleet. Its rank was stable across sensitivity analyses (first to fourth when indicators were left out, third with an arithmetic mean), whereas Lethabo ranged from first to tenth and Duvha from second to fourteenth, because their high exposure scores were offset by low vulnerability. Morupule had high vulnerability but the weakest pollution signal of the detectable plants.

This manuscript is a preprint and has not been peer reviewed. The copyright holder has made the manuscript available under a Creative Commons Attribution 4.0 International (CC BY) license and consented to have it forwarded to EarthArXiv for public posting.

The spatial distribution of compound risk shows where these components overlap (Figs 7 and 8). Around Hwange, high-index cells form a continuous zone over the town and its surroundings, and 20,700 people, 38% of those within 50 km, live in cells in the top decile of the pooled index. Around the South African plants, the corresponding share was 0.2 to 9.6%, and around Lethabo, the highest-ranked plant overall, only 0.2%, because its large population lives close to health care and in a cooler climate.

The continuous risk surface shows that compound risk is not confined to the plant sites (Fig. 8). It forms broad high-risk zones across the Highveld cluster and around Hwange town, whereas the Lephalale pair and Morupule sit in largely low-risk surroundings. The population-weighted risk within 25 km was highest near Komati (0.50) and Hwange (0.49), and lowest near Camden (0.23); Lethabo, first on the plant-level index because of its population, scored 0.26.

This manuscript is a preprint and has not been peer reviewed. The copyright holder has made the manuscript available under a Creative Commons Attribution 4.0 International (CC BY) license and consented to have it forwarded to EarthArXiv for public posting.

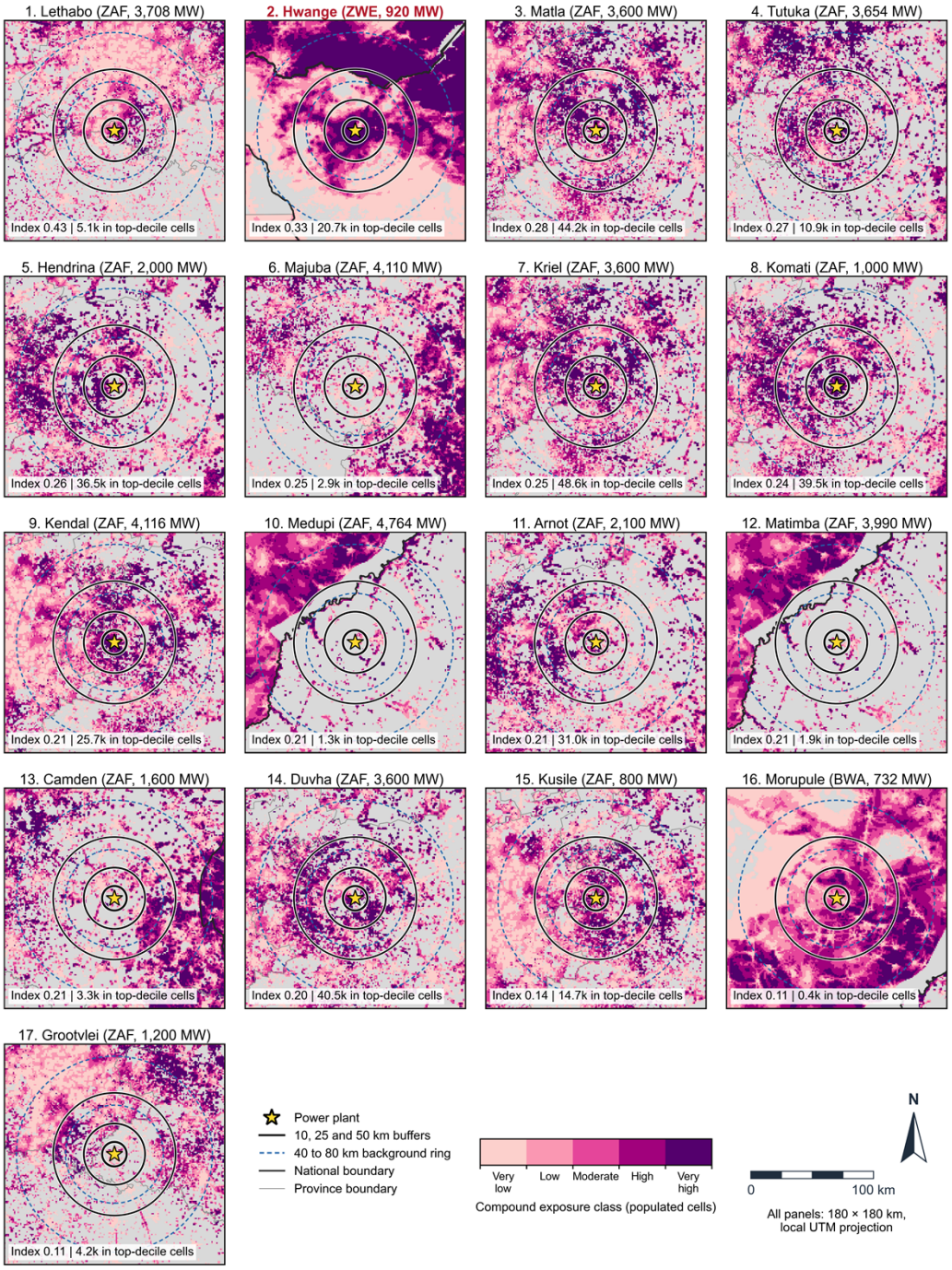


Fig 7. Spatial distribution of compound exposure around each detectable plant. *Cell-level compound index (Eq. 5) for populated 1 km cells, combining NO_2, night heat anomaly, population density, and travel time to health care as percentile ranks pooled across all plants. Labels give the plant-level index and the number of people within 50 km who live in top-decile cells. Cells are shown in five classes split at the quintiles of all plants (very low to very high); unpopulated cells are grey.*

This manuscript is a preprint and has not been peer reviewed. The copyright holder has made the manuscript available under a Creative Commons Attribution 4.0 International (CC BY) license and consented to have it forwarded to EarthArXiv for public posting.

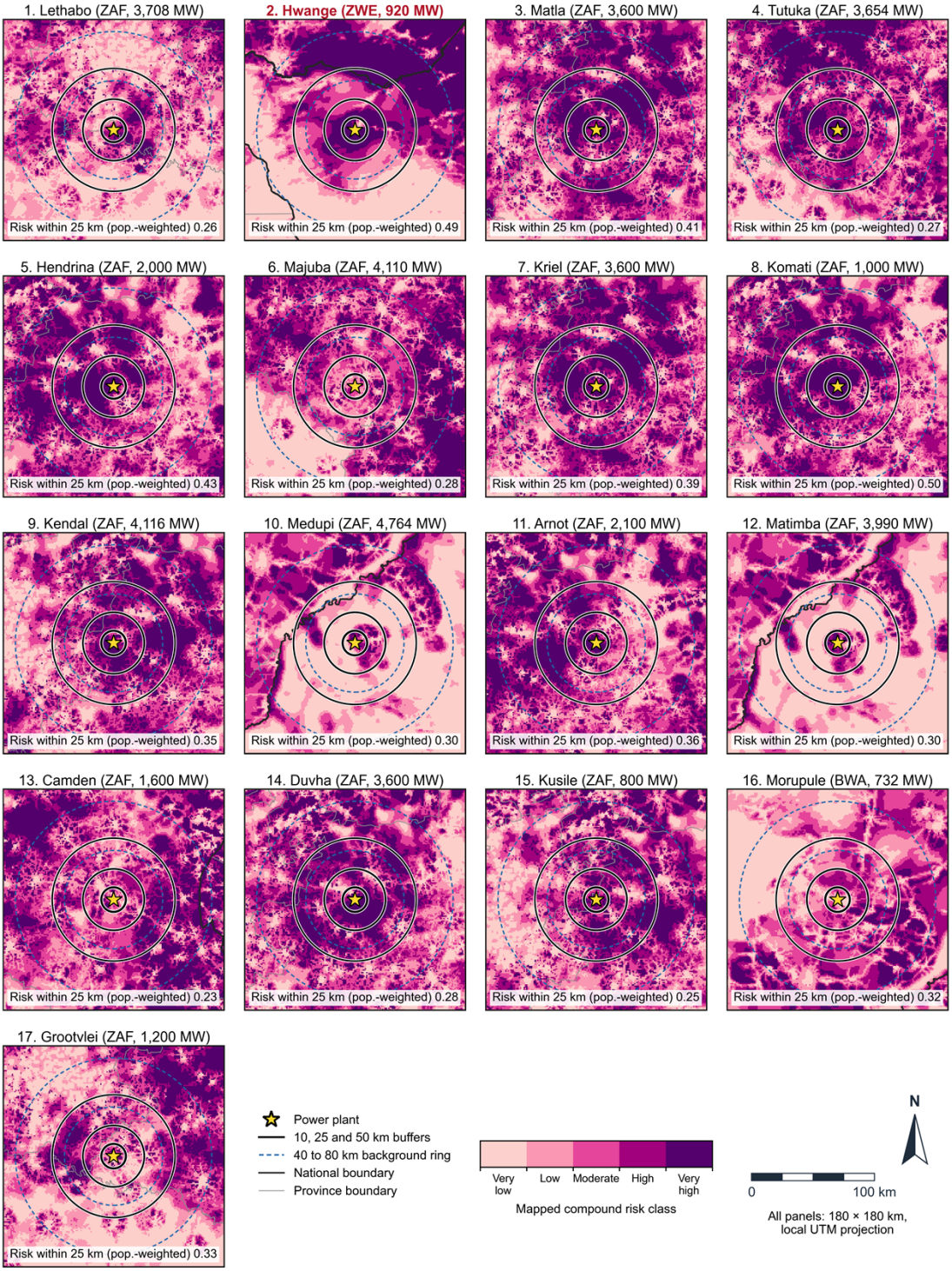


Fig 8. Mapped compound risk around each detectable plant. *Continuous compound risk surface for every 1 km cell: geometric mean of hazard (NO_2 and night heat percentiles), exposure (population within reach, density smoothed with a Gaussian kernel of 3 km) and vulnerability (travel time to health care), with percentiles pooled over all cells of the 17 windows, shown in five quintile classes from very low to very high. Labels give the population-weighted risk within 25 km.*

This manuscript is a preprint and has not been peer reviewed. The copyright holder has made the manuscript available under a Creative Commons Attribution 4.0 International (CC BY) license and consented to have it forwarded to EarthArXiv for public posting.

5 Discussion

5.1 A shifting coal frontier

Coal pollution in southern Africa is moving. Most South African stations emitted less after mid-2023, consistent with the fleet's low availability during years of breakdowns and load shedding. (Council for Scientific and Industrial Research, 2025), whereas the NO_2 excess around Hwange rose by about four-fifths and the SO_2 excess doubled after Units 7 and 8 came online. The increase was immediate, persisted for more than three years, survived adjustment for season and trend, and was the largest in the fleet. The new units were built partly to cover hydropower shortfalls on the Zambezi, where the Kariba catchment shows marked hydroclimatic variability and generation was capped during the 2022 drought (Al Jazeera, 2022; Conway et al., 2017; Mwangala et al., 2024). Climate stress on the energy system has therefore been converted into additional air pollution for nearby residents. Hwange is a modest emitter by Highveld standards, but this does not make its growth unimportant: in the United States, fine particles formed from coal power plant sulphur dioxide carried 2.1 times the mortality risk of fine particles from all sources (Henneman et al., 2023), and the doubling of the SO_2 excess at Hwange points to more of this secondary particulate pollution downwind.

5.2 Where pollution meets heat

Hwange is also where the new pollution meets the most heat. Residents experience about two months a year above 35 °C; the town is the strongest night-time heat island of any detectable plant, and the pollution excess peaked in 2024, the year with the most

This manuscript is a preprint and has not been peer reviewed. The copyright holder has made the manuscript available under a Creative Commons Attribution 4.0 International (CC BY) license and consented to have it forwarded to EarthArXiv for public posting.

hot days in our series. Multi-country studies show that heat effects on cardiorespiratory mortality are stronger when particulate and gaseous pollution are high, and that pollution effects are stronger on hot days (Anenberg et al., 2020). Long-term NO_2 exposure is itself associated with higher mortality, with high certainty for chronic obstructive pulmonary disease and lower respiratory infections (X. Chen et al., 2024; Kasdagli et al., 2024). African evidence on these combined exposures is thin: a 2026 systematic review found that only three African case-control studies of air pollution and respiratory health included temperature and none examined heat and pollution together (Wright et al., 2026), and a decade of time-series data from Limpopo, the province of the Lephalale plants, links ambient pollution to cardiovascular and respiratory deaths (Opiyo et al., 2026). The overlap of pollution and heat that our maps reveal around Hwange and Lephalale is therefore a gap in evidence as well as a hazard.

5.3 Unequal exposure and vulnerability

The contrast with the Highveld shows why single-pollutant rankings mislead. The Mpumalanga stations emit far more and sit within larger populations, and they dominate rankings of pollution or exposure. Their residents, however, experience almost no days above 35 °C and live within minutes of a health facility. People near Hwange, and to a lesser extent near Morupule and the Lephalale plants, face the same kinds of exposure with longer journeys to care and fewer resources to adapt (Fisher et al., 2021; Weiss et al., 2020). At the cell level, this difference is stark: more than a third of residents within 50 km of Hwange live in the top decile of compound risk, compared with at most one in ten around any South African plant. Considering exposures together rather than one at

This manuscript is a preprint and has not been peer reviewed. The copyright holder has made the manuscript available under a Creative Commons Attribution 4.0 International (CC BY) license and consented to have it forwarded to EarthArXiv for public posting.

a time is the central argument of the exposome approach (Vermeulen et al., 2020; Wild, 2005), and the absence of continuous monitoring near African emission sources has been described as a form of environmental injustice (Jenkins, 2025). Our results suggest that the communities on the expanding frontier are the least protected on both counts.

5.4 Implications for monitoring, policy and research

New coal units in hot, drought-exposed areas should come with emission controls, ground-level monitoring of NO_2, SO_2 and $PM_{2.5}$ in nearby towns, and heat and air quality alerts that are issued together. Health services in Hwange district could plan for respiratory and cardiovascular demand in the hottest months. Satellite observations from Sentinel-5P and newer missions are now mature enough to support routine surveillance of such sources (Beirle et al., 2019; Stratoulias et al., 2024), and because our approach uses only open data, it can be repeated as Maamba's second phase (Zambia Monitor, 2024) and other planned units come online. The next step is to link these hazard maps with ground monitoring and routine health records around Hwange, so that the compound exposures identified here can be related to measured health outcomes (Achakulwisut et al., 2019; Khreis et al., 2017)

5.5 Strengths and limitations

The study combines a fleet-wide screen with a quasi-experimental evaluation, uses a local background to remove regional influences, counts shared populations once, and reports every sensitivity analysis. It has important limitations. TROPOMI measures

This manuscript is a preprint and has not been peer reviewed. The copyright holder has made the manuscript available under a Creative Commons Attribution 4.0 International (CC BY) license and consented to have it forwarded to EarthArXiv for public posting.

columns, not concentrations at breathing height, and the excess around a plant includes co-located sources such as towns, coal mines, coking plants, and traffic; at Hwange these operations are part of the same coal economy, and at Lethabo the Vaal industries contribute. The NO_2 signal also depends on wind, sunlight, and chemistry, and we did not estimate emissions with flux methods. Monthly generation data for Hwange are not public, so we could not relate the satellite signal to output directly. The plant list is several years old, and the small Bulawayo, Harare and Munyati stations in Zimbabwe were not included. $PM_{2.5}$ data ended in 2022, so the mortality contrasts describe the baseline and are conditional on transferring functions from other populations. The 35 °C threshold is an absolute marker of hot days and not a locally derived health threshold. Finally, the index is relative to the plants included, and its weights are a choice; we addressed this with alternative formulations. The cell-level index uses percentile ranks pooled across all plants, so it describes relative rather than absolute risk.

6 Conclusions

Coal pollution in southern Africa is declining at its traditional center and rising at its frontier. At Hwange, new units commissioned in 2023 increased NO_2 and SO_2 around a town that is among the hottest and least served of any coal plant community in the region, and Hwange ranks second for compound pollution and heat risk. Open satellite and population data can identify such places early. Energy planning in the Zambezi basin should treat air quality, heat and health as part of the cost of new coal capacity.

This manuscript is a preprint and has not been peer reviewed. The copyright holder has made the manuscript available under a Creative Commons Attribution 4.0 International (CC BY) license and consented to have it forwarded to EarthArXiv for public posting.

6.1 Acknowledgments

We thank the providers of the open datasets used in this study: ESA and KNMI (TROPOMI), ECMWF (ERA5-Land), NASA (MODIS and FIRMS), WorldPop, the Malaria Atlas Project, the GHAP team, the World Resources Institute and the World Bank.

6.2 Funding

This research received no external funding.

6.3 Competing interests

The authors have declared that no competing interests exist.

6.4 Author contributions

Handsome Bongani Nyoni and Rutendo Mandeya conceptualized the study. Handsome Bongani Nyoni led data curation, investigation, methodological development, formal analysis, software development, and visualization. Rutendo Mandeya, Zororo Kudzai Chinwadzimba and Rutendo Sibanda contributed to formal analysis and visualization. Daniel Tigere, Perez Livias Moyo and Webster Gumindoga contributed to methodology and validation. Handsome Bongani Nyoni, Rutendo Sibanda and Daniel Tigere contributed to preparing the original manuscript. All authors contributed to manuscript review and editing.

6.5 Data availability

The code and derived datasets that support this study are openly available. Version 1.0.0 of the analysis code (Python) and the derived datasets (plant-level annual and monthly NO_2 and SO_2 tables, heat, population, $PM_{2.5}$ and health care access indicators, the compound risk index and the statistical results) are archived at Zenodo (Nyoni et al.,

This manuscript is a preprint and has not been peer reviewed. The copyright holder has made the manuscript available under a Creative Commons Attribution 4.0 International (CC BY) license and consented to have it forwarded to EarthArXiv for public posting.

2026b), https://doi.org/10.5281/zenodo.23367004, under the MIT licence (code) and CC BY 4.0 (derived datasets), and are maintained at https://github.com/Hbnyoni/-hwange-coal-frontiers. Large raster extracts are not redistributed; the archived scripts require them from the public sources listed here. All inputs are public: Sentinel-5P TROPOMI tropospheric NO_2 and SO_2 offline level 3 products https://developers.google.com/earth engine/datasets/catalog/-COPERNICUS_S5P_OFFL_L3_NO_2 and https://developers.-google.com/earth-engine/datasets/-catalog/-COPERNICUS_-S5P_OFFL_L3_-SO_2 ERA5-Land daily and monthly aggregateshttps://developers.google.com/earth-engine/datasets/catalog/-ECMWF_ERA5_LAND_-DAILY_AGGR, MODIS MOD11A2 version 6.1 land surface temperature https://developers.google.com/earth-engine-/datasets-/catalog/MODIS_061_MOD11A2) ; FIRMS active fires (https://developers-.google.com/earth-engine/datasets/catalog/FIRMS); WorldPop 2020 population and age and sex structure https://developers.google.com/earth-engine-/datasets/-catalog/WorldPop_GP_100m_pop); the Malaria Atlas Project travel time to health care, 2019https://developers.google.com/earth-engine/datasets/-catalog/Oxford_MAP-_accessibility_to_healthcare_2019, accessed through its successor asset projects/malariaatlasproject/assets/accessibility/accessibility_to_healthcare/2019); GHAP $PM_{2.5}$ (https://gee-community-catalog.org/projects/ghap/); the Global Power Plant Database version 1.3.0https://datasets.wri.org/dataset/globalpowerplantdatabase); geoBoundaries gbOpen boundaries, commit 9469f09 https://github.com/wmgeolab-/geoBoundaries/tree/9469f09); World Bank crude death rates https://data.-worldbank.org/indicator/SP.DYN.CDRT.IN) ; and Natural Earth physical layers

This manuscript is a preprint and has not been peer reviewed. The copyright holder has made the manuscript available under a Creative Commons Attribution 4.0 International (CC BY) license and consented to have it forwarded to EarthArXiv for public posting.

(https://www.naturalearthdata.com). Earth Engine access requires a free registered account. No new human, survey, or clinical data were collected.

7 References

Abadie, A., Diamond, A., & Hainmueller, J. (2010). Synthetic control methods for comparative case studies: Estimating the effect of california's tobacco control program. *Journal of the American Statistical Association*, *105*(490), 493–505. https://doi.org/10.1198/jasa.2009.ap08746

Achakulwisut, P., Brauer, M., Hystad, P., & Anenberg, S. C. (2019). Global, national, and urban burdens of paediatric asthma incidence attributable to ambient NO2 pollution: Estimates from global datasets. *The Lancet Planetary Health*, *3*(4), e166–e178. https://doi.org/10.1016/S2542-5196(19)30046-4

Al Jazeera. (2022, December 2). Zambia plans power cuts due to low water levels in Lake Kariba. *Al Jazeera*. https://www.aljazeera.com/news/2022/12/2/zambia-plans-power-cuts-dulow-levels

Anenberg, S. C., Haines, S., Wang, E., Nassikas, N., & Kinney, P. L. (2020). Synergistic health effects of air pollution, temperature, and pollen exposure: A systematic review of epidemiological evidence. *Environmental Health*, *19*(1), 130. https://doi.org/10.1186/s12940-020-00681-z

Beirle, S., Borger, C., Dörner, S., Li, A., Hu, Z., Liu, F., Wang, Y., & Wagner, T. (2019). Pinpointing nitrogen oxide emissions from space. *Science Advances*, *5*(11), eaax9800. https://doi.org/10.1126/sciadv.aax9800

This manuscript is a preprint and has not been peer reviewed. The copyright holder has made the manuscript available under a Creative Commons Attribution 4.0 International (CC BY) license and consented to have it forwarded to EarthArXiv for public posting.

Chen, J., & Hoek, G. (2020). Long-term exposure to PM and all-cause and cause-specific mortality: A systematic review and meta-analysis. *Environment International*, *143*, 105974. https://doi.org/10.1016/j.envint.2020.105974

Chen, X., Qi, L., Li, S., & Duan, X. (2024). Long-term NO2 exposure and mortality: A comprehensive meta-analysis. *Environmental Pollution*, *341*, 122971. https://doi.org/10.1016/j.envpol.2023.122971

Conway, D., Dalin, C., Landman, W. A., & Osborn, T. J. (2017). Hydropower plans in eastern and southern Africa increase risk of concurrent climate-related electricity supply disruption. *Nature Energy*, *2*(12), 946–953. https://doi.org/10.1038/s41560-017-0037-4

Council for Scientific and Industrial Research. (2025). *Utility statistics report: January 2025*. CSIR. https://www.csir.co.za/sites/default/files/2025-11/UtilityStatisticsReportJan2025Final.pdf

Fisher, S., Bellinger, D. C., Cropper, M. L., Kumar, P., Binagwaho, A., Koudenoukpo, J. B., Park, Y., Taghian, G., & Landrigan, P. J. (2021). Air pollution and development in Africa: Impacts on health, the economy, and human capital. *The Lancet Planetary Health*, *5*(10), e681–e688. https://doi.org/10.1016/S2542-5196(21)00201-1

Global Energy Monitor. (2024). *Boom and bust coal 2024: Tracking the global coal plant pipeline*. https://globalenergymonitor.org/report/boom-and-bust-coal-2024/

Global Energy Observatory, Google, KTH Royal Institute of Technology in Stockholm, Enipedia, & World Resources Institute. (2021). *Global power plant database* (Version 1.3.0) [Dataset]. World Resources Institute. https://datasets.wri.org/dataset/globalpowerplantdatabase

This manuscript is a preprint and has not been peer reviewed. The copyright holder has made the manuscript available under a Creative Commons Attribution 4.0 International (CC BY) license and consented to have it forwarded to EarthArXiv for public posting.

599 Goldberg, D. L., Lu, Z., Streets, D. G., de Foy, B., Griffin, D., McLinden, C. A., Lamsal, L. N.,
600 Krotkov, N. A., & Eskes, H. (2019). Enhanced capabilities of TROPOMI NO2:
601 Estimating NOx from North American cities and power plants. *Environmental Science &*
602 *Technology*, *53*(21), 12594–12601. https://doi.org/10.1021/acs.est.9b04488
603 Gorelick, N., Hancher, M., Dixon, M., Ilyushchenko, S., Thau, D., & Moore, R. (2017). Google
604 Earth Engine: Planetary-scale geospatial analysis for everyone. *Remote Sensing of*
605 *Environment*, *202*, 18–27. https://doi.org/10.1016/j.rse.2017.06.031
606 Henneman, L., Choirat, C., Dedoussi, I., Dominici, F., Roberts, J., & Zigler, C. (2023). Mortality
607 risk from united states coal electricity generation. *Science*, *382*(6673), 941–946.
608 https://doi.org/10.1126/science.adf4915
609 IPCC. (2022). Summary for policymakers. In H.-O. Portner, D. C. Roberts, E. S. Poloczanska,
610 K. Mintenbeck, M. Tignor, A. Alegría, M. Craig, S. Langsdorf, S. Löschke, V. Möller, &
611 A. Okem (Eds.), *Climate change 2022: Impacts, adaptation and vulnerability.*
612 *Contribution of Working Group II to the Sixth Assessment Report of the*
613 *Intergovernmental Panel on Climate Change* (pp. 3–33). Cambridge University Press.
614 https://doi.org/10.1017/9781009325844.001
615 Jenkins, G. S. (2025). The lack of Real-Time air pollution monitoring in Africa supports
616 environmental injustice. *Environmental Justice*, *18*(2), 85–89.
617 https://doi.org/10.1089/env.2023.0030
618 Kasdagli, M.-I., Orellano, P., Pérez Velasco, R., & Samoli, E. (2024). Long-Term exposure to
619 nitrogen dioxide and ozone and mortality: Update of the WHO air quality guidelines
620 systematic review and Meta-Analysis. *International Journal of Public Health*, *69*,
621 1607676. https://doi.org/10.3389/ijph.2024.1607676

This manuscript is a preprint and has not been peer reviewed. The copyright holder has made the manuscript available under a Creative Commons Attribution 4.0 International (CC BY) license and consented to have it forwarded to EarthArXiv for public posting.

Khreis, H., Kelly, C., Tate, J., Parslow, R., Lucas, K., & Nieuwenhuijsen, M. (2017). Exposure to traffic-related air pollution and risk of development of childhood asthma: A systematic review and meta-analysis. *Environment International*, *100*, 1–31. https://doi.org/10.1016/j.envint.2016.11.012

Lopez Bernal, J., Cummins, S., & Gasparrini, A. (2017). Interrupted time series regression for the evaluation of public health interventions: A tutorial. *International Journal of Epidemiology*, *46*(1), 348–355. https://doi.org/10.1093/ije/dyw098

Mining Index. (2023a, May). All set for Hwange Unit 8 synchronisation on 16 May. *Mining Index Zimbabwe*. https://www.miningindex.co.zw/?p=24926

Mining Index. (2023b, June). Update: Hwange Power Station's Unit 8 synchronised to national grid. *Mining Index Zimbabwe*. https://www.miningindex.co.zw/?p=25110

Muñoz-Sabater, J., Dutra, E., Agustí-Panareda, A., Albergel, C., Arduini, G., Balsamo, G., Boussetta, S., Choulga, M., Harrigan, S., Hersbach, H., Martens, B., Miralles, D. G., Piles, M., Rodríguez-Fernández, N. J., Zsoter, E., Buontempo, C., & Thépaut, J.-N. (2021). ERA5-Land: A state-of-the-art global reanalysis dataset for land applications. *Earth System Science Data*, *13*(9), 4349–4383. https://doi.org/10.5194/essd-13-4349-2021

Mwangala, B. B., Banda, K., Chimuka, L., Uchida, Y., & Nyambe, I. (2024). Analysis of streamflow and rainfall trends and variability over the lake kariba catchment, upper zambezi basin. *Hydrology Research*, *55*(7), 683–710. https://doi.org/10.2166/nh.2024.122

This manuscript is a preprint and has not been peer reviewed. The copyright holder has made the manuscript available under a Creative Commons Attribution 4.0 International (CC BY) license and consented to have it forwarded to EarthArXiv for public posting.

Newey, W. K., & West, K. D. (1987). A simple, positive Semi-Definite, heteroskedasticity and autocorrelation consistent covariance matrix. *Econometrica*, *55*(3), 703–708. https://doi.org/10.2307/1913610

Nyoni, H. B., Moyo, P. L., Chinwadzimba, Z., Sibanda, R., & Tigere, D. (2026). *Midlands PM2.5 population exposure and health risk profiles: Code and derived data* (Version 1.0.0) [Computer software]. Zenodo. https://doi.org/10.5281/zenodo.23342801

OECD & European Commission Joint Research Centre. (2008). *Handbook on constructing composite indicators: Methodology and user guide*. OECD Publishing. https://doi.org/10.1787/9789264043466-en

Opiyo, S. B., Burger, R., Balaka, M. N., & Piketh, S. (2026). Air pollution and cardio-respiratory mortality in limpopo, south Africa (2011–2020): Evidence on population and seasonal vulnerability. *Air Quality, Atmosphere & Health*, *19*(6), 127. https://doi.org/10.1007/s11869-026-02022-4

Python Software Foundation. (2024). *Python* (Version 3.12) [Computer software]. https://www.python.org/

R Core Team. (2024). *R: A language and environment for statistical computing* (Version 4.4.2) [Computer software]. R Foundation for Statistical Computing. https://www.R-project.org/

Rai, M., Stafoggia, M., de'Donato, F., Scortichini, M., Zafeiratou, S., Vazquez Fernandez, L., Zhang, S., Katsouyanni, K., Samoli, E., Rao, S., Lavigne, E., Guo, Y., Kan, H., Osorio, S., Kyselý, J., Urban, A., Orru, H., Maasikmets, M., Jaakkola, J. J., & Breitner, S. (2023). Heat-related cardiorespiratory mortality: Effect modification by air pollution across 482

This manuscript is a preprint and has not been peer reviewed. The copyright holder has made the manuscript available under a Creative Commons Attribution 4.0 International (CC BY) license and consented to have it forwarded to EarthArXiv for public posting.

cities from 24 countries. *Environment International*, *174*, 107825. https://doi.org/10.1016/j.envint.2023.107825

Romanello, M., Walawender, M., Hsu, S.-C., Moskeland, A., Palmeiro-Silva, Y., Scamman, D., Ali, Z., Ameli, N., Angelova, D., Ayeb-Karlsson, S., Basart, S., Beagley, J., Beggs, P. J., Blanco-Villafuerte, L., Cai, W., Callaghan, M., Campbell-Lendrum, D., Chambers, J. D., Chicmana-Zapata, V., & Costello, A. (2024). The 2024 report of the Lancet Countdown on health and climate change: Facing record-breaking threats from delayed action. *The Lancet*, *404*(10465), 1847–1896. https://doi.org/10.1016/S0140-6736(24)01822-1

Runfola, D., Anderson, A., Baier, H., Crittenden, M., Dowker, E., Fuhrig, S., Goodman, S., Grimsley, G., Layko, R., Melville, G., Mulder, M., Oberman, R., Panganiban, J., Peck, A., Seitz, L., Shea, S., Slevin, H., Youngerman, R., & Hobbs, L. (2020). GeoBoundaries: A global database of political administrative boundaries. *PLOS ONE*, *15*(4), e0231866. https://doi.org/10.1371/journal.pone.0231866

Stafoggia, M., Michelozzi, P., Schneider, A., Armstrong, B., Scortichini, M., Rai, M., Achilleos, S., Alahmad, B., Analitis, A., Åström, C., Bell, M. L., Calleja, N., Krage Carlsen, H., Carrasco, G., Paul Cauchi, J., DSZS Coelho, M., Correa, P. M., Diaz, M. H., Entezari, A., & de' Donato, F. K. (2023). Joint effect of heat and air pollution on mortality in 620 cities of 36 countries. *Environment International*, *181*, 108258. https://doi.org/10.1016/j.envint.2023.108258

Stratoulias, D., Nuthammachot, N., Dejchanchaiwong, R., Tekasakul, P., & Carmichael, G. R. (2024). Recent developments in satellite remote sensing for air pollution surveillance in support of sustainable development goals. *Remote Sensing*, *16*(16), 2932. https://doi.org/10.3390/rs16162932

This manuscript is a preprint and has not been peer reviewed. The copyright holder has made the manuscript available under a Creative Commons Attribution 4.0 International (CC BY) license and consented to have it forwarded to EarthArXiv for public posting.

Tatem, A. J. (2017). WorldPop, open data for spatial demography. *Scientific Data*, *4*(1), 170004. https://doi.org/10.1038/sdata.2017.4

Techzim. (2023, June). Hwange Unit 8 to contribute 300MW to the grid before June is up, Unit 7 already there. *Techzim*. https://techzim.co.zw/2023/06/hwange-unit-8-to-contribute-300mw-to-grid-in-june-unit-7-already-there

The Southern, E. (2024). *Hwange residents petition NSSA over respiratory diseases stats—The Southern Eye*. Southern Eye. Southern Eye. https://www.southerneye.co.zw/local/article/200032482/hwange-residents-petition-nssa-over-respiratory-diseases-stats

Theys, N., De Smedt, I., Yu, H., Danckaert, T., van Gent, J., Hörmann, C., Wagner, T., Hedelt, P., Bauer, H., Romahn, F., Pedergnana, M., Loyola, D., & Van Roozendael, M. (2017). Sulfur dioxide retrievals from TROPOMI onboard Sentinel-5 Precursor: Algorithm theoretical basis. *Atmospheric Measurement Techniques*, *10*(1), 119–153. https://doi.org/10.5194/amt-10-119-2017

van Geffen, J., Eskes, H., Compernolle, S., Pinardi, G., Verhoelst, T., Lambert, J.-C., Sneep, M., ter Linden, M., Ludewig, A., Boersma, K. F., & Veefkind, J. P. (2022). Sentinel-5P TROPOMI NO2 retrieval: Impact of version v2.2 improvements and comparisons with OMI and ground-based data. *Atmospheric Measurement Techniques*, *15*(7), 2037–2060. https://doi.org/10.5194/amt-15-2037-2022

Veefkind, J., Aben, I., McMullan, K., Förster, H., de Vries, J., Otter, G., Claas, J., Eskes, H., de Haan, J., Kleipool, Q., van Weele, M., Hasekamp, O., Hoogeveen, R., Landgraf, J., Snel, R., Tol, P., Ingmann, P., Voors, R., Kruizinga, B., & Levelt, P. (2012). TROPOMI on the ESA Sentinel-5 Precursor: A GMES mission for global observations of the atmospheric

This manuscript is a preprint and has not been peer reviewed. The copyright holder has made the manuscript available under a Creative Commons Attribution 4.0 International (CC BY) license and consented to have it forwarded to EarthArXiv for public posting.

composition for climate, air quality and ozone layer applications. *Remote Sensing of Environment*, *120*, 70–83. https://doi.org/10.1016/j.rse.2011.09.027

Vermeulen, R., Schymanski, E. L., Barabási, A.-L., & Miller, G. W. (2020). The exposome and health: Where chemistry meets biology. *Science*, *367*(6476), 392–396. https://doi.org/10.1126/science.aay3164

Wan, Z. (2014). New refinements and validation of the collection-6 MODIS land-surface temperature/emissivity product. *Remote Sensing of Environment*, *140*, 36–45. https://doi.org/10.1016/j.rse.2013.08.027

Wei, J., Li, Z., Lyapustin, A., Wang, J., Dubovik, O., Schwartz, J., Sun, L., Li, C., Liu, S., & Zhu, T. (2023). First close insight into global daily gapless 1 km PM2.5 pollution, variability, and health impact. *Nature Communications*, *14*(1), 8349. https://doi.org/10.1038/s41467-023-43862-3

Weiss, D. J., Nelson, A., Vargas-Ruiz, C. A., Gligorić, K., Bavadekar, S., Gabrilovich, E., Bertozzi-Villa, A., Rozier, J., Gibson, H. S., Shekel, T., Kamath, C., Lieber, A., Schulman, K., Shao, Y., Qarkaxhija, V., Nandi, A. K., Keddie, S. H., Rumisha, S., Amratia, P., & Gething, P. W. (2020). Global maps of travel time to healthcare facilities. *Nature Medicine*, *26*(12), 1835–1838. https://doi.org/10.1038/s41591-020-1059-1

Wild, C. P. (2005). Complementing the genome with an “exposome”: The outstanding challenge of environmental exposure measurement in molecular epidemiology. *Cancer Epidemiology, Biomarkers & Prevention*, *14*(8), 1847–1850. https://doi.org/10.1158/1055-9965.EPI-05-0456

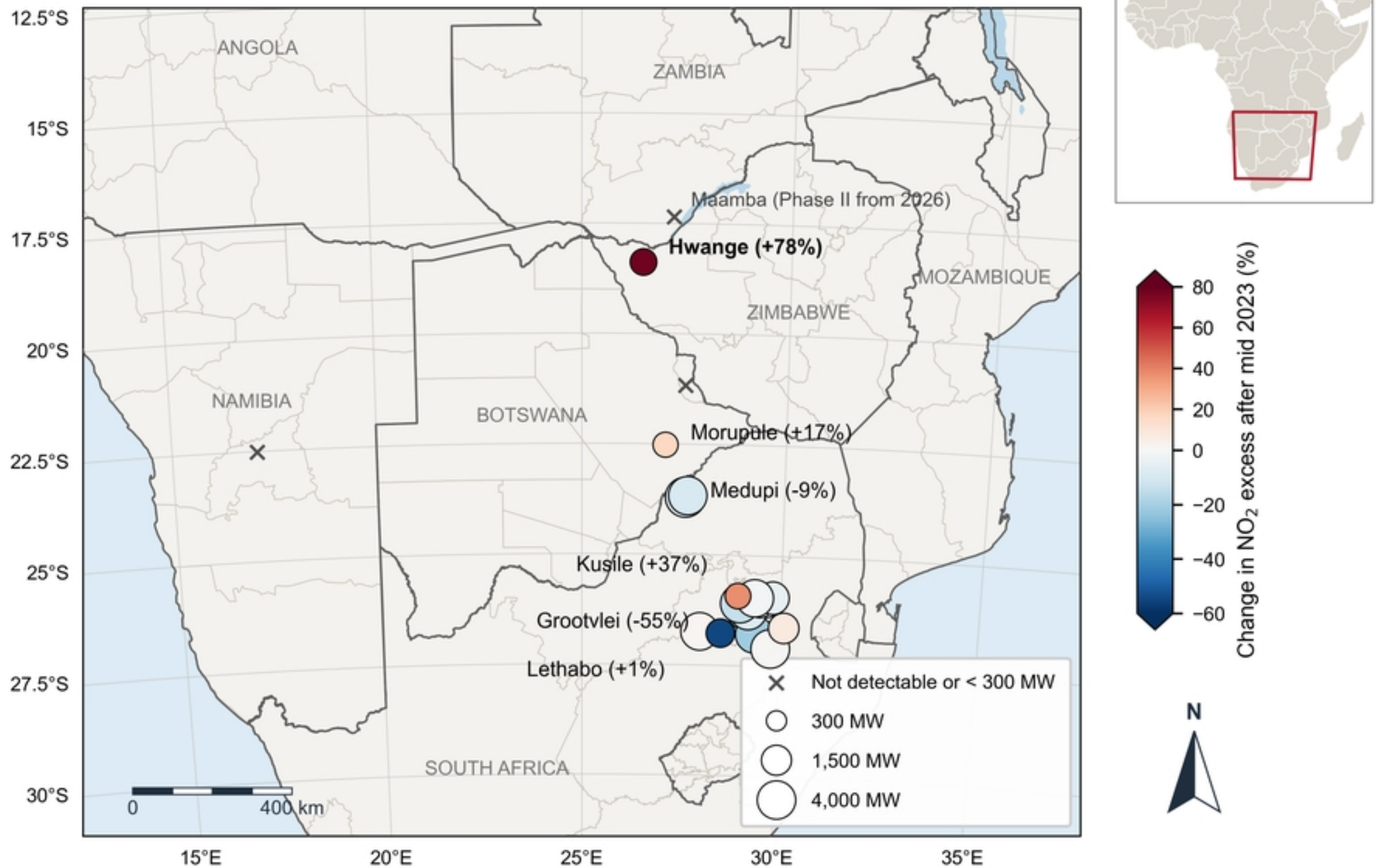
This manuscript is a preprint and has not been peer reviewed. The copyright holder has made the manuscript available under a Creative Commons Attribution 4.0 International (CC BY) license and consented to have it forwarded to EarthArXiv for public posting.

World Bank. (2026). Death rate, crude (per 1,000 people) (Indicator SP.DYN.CDRT.IN) [Dataset]. In *World Development Indicators*. https://data.worldbank.org/indicator/SP.DYN.CDRT.IN

World Health Organization. (2021). *WHO global air quality guidelines: Particulate matter (PM2.5 and PM10), ozone, nitrogen dioxide, sulfur dioxide and carbon monoxide*. https://www.who.int/publications/i/item/9789240034228

Wright, C. Y., Kapwata, T., Dikoko, V., Howlett-Downing, C., & Naidoo, N. (2026). Air pollution and heat impacts on respiratory morbidity and mortality outcomes in Africa: A systematic review towards a meta-analysis. *Current Environmental Health Reports*, *13*(1), 39. https://doi.org/10.1007/s40572-026-00561-7

Zambia Monitor. (2024). Maamba Collieries secures financing for $400 million power plant expansion. *Zambia Monitor*. https://zambiamonitor.com/maamba-collieries-secures-financing-for-400-million-power-plant-expansion



Boundaries: geoBoundaries gbOpen ADM0 and ADM1 (commit 9469f09); ocean, lakes and locator: Natural Earth. Lambert azimuthal equal-area projection (25°E, 22°S).

Figure 1

This manuscript is a preprint and has not been peer-reviewed. The copyright holder has made the manuscript available under a Creative Commons Attribution 4.0 International (CC BY) license and consented to have it forwarded to EarthArXiv for public posting.

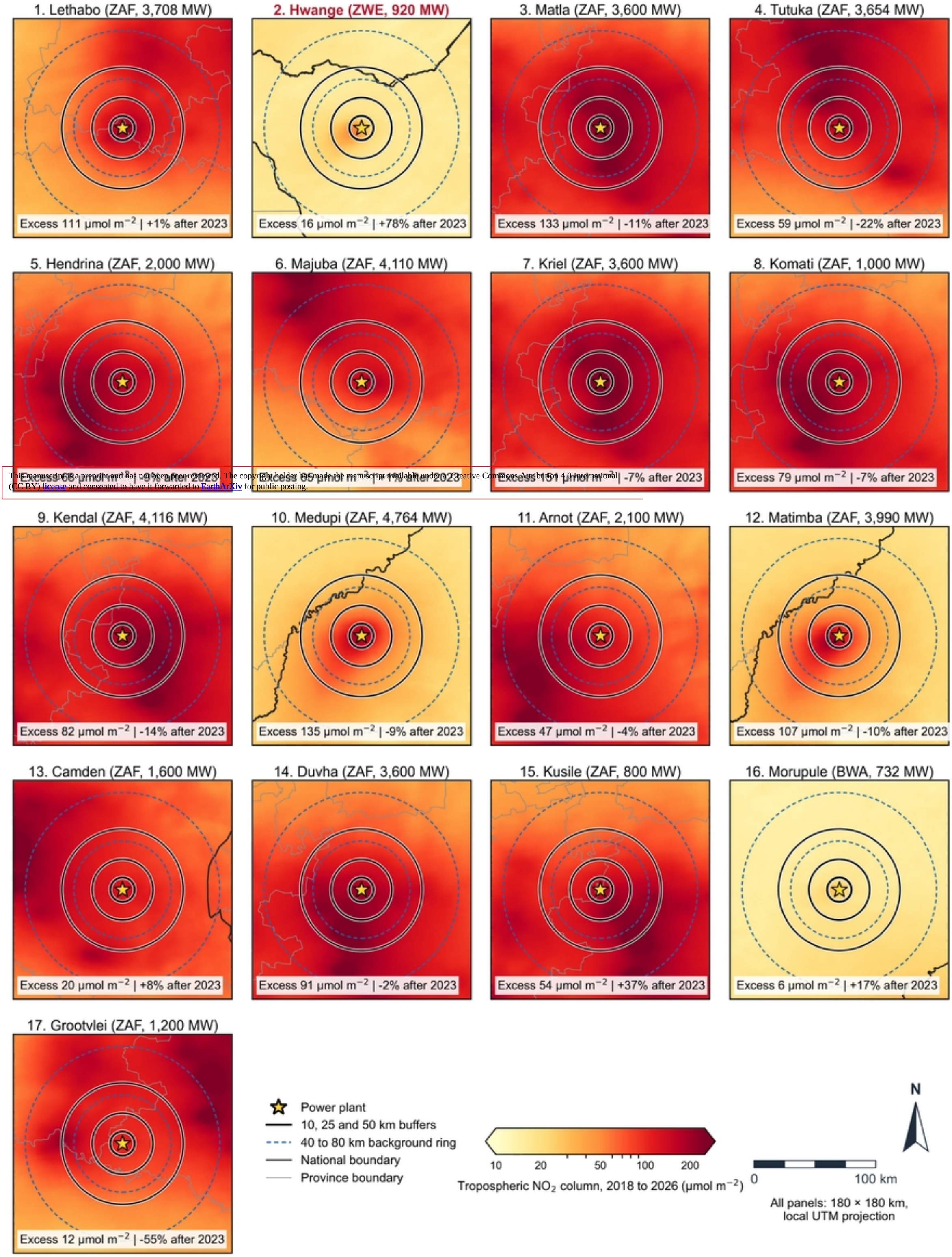


Figure 2

This manuscript is a preprint and has not been peer reviewed. The copyright holder has made the manuscript available under a Creative Commons Attribution 4.0 International (CC BY) license and consented to have it forwarded to EarthArXiv for public posting.

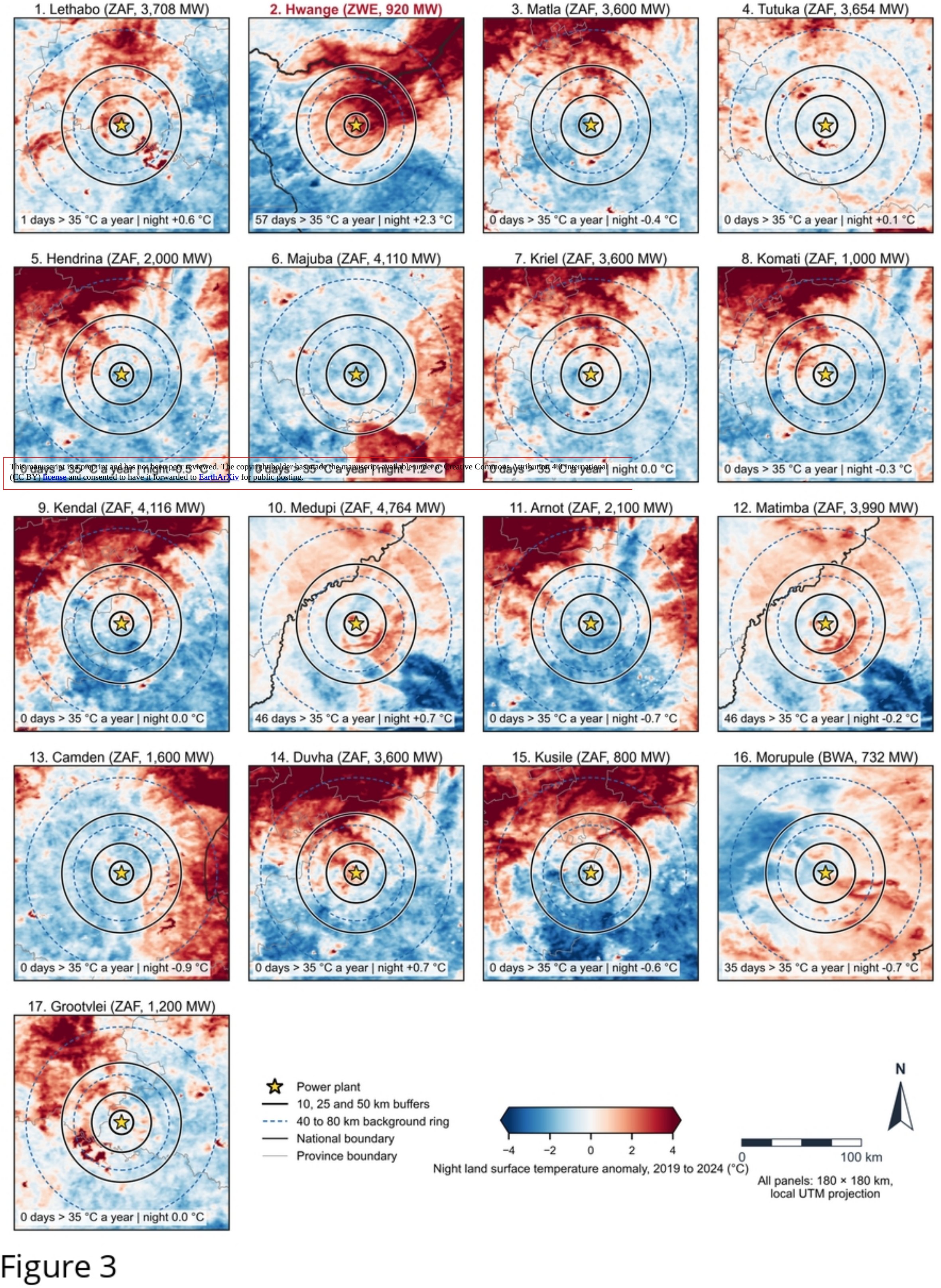


Figure 3

This manuscript is a preprint and has not been peer reviewed. The copyright holder has made the manuscript available under a Creative Commons Attribution 4.0 International (CC BY) license and consented to have it forwarded to EarthArXiv for public posting.

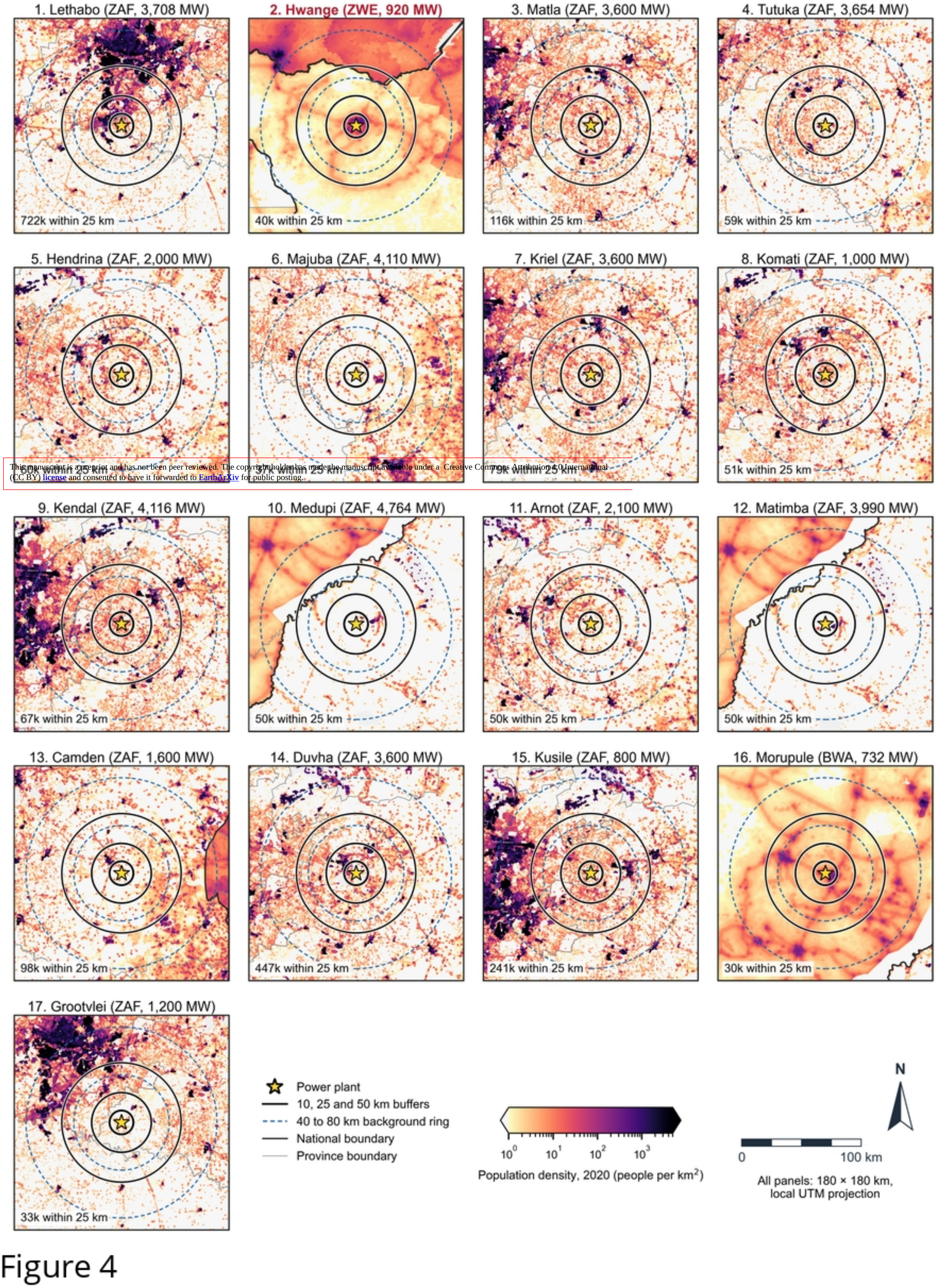
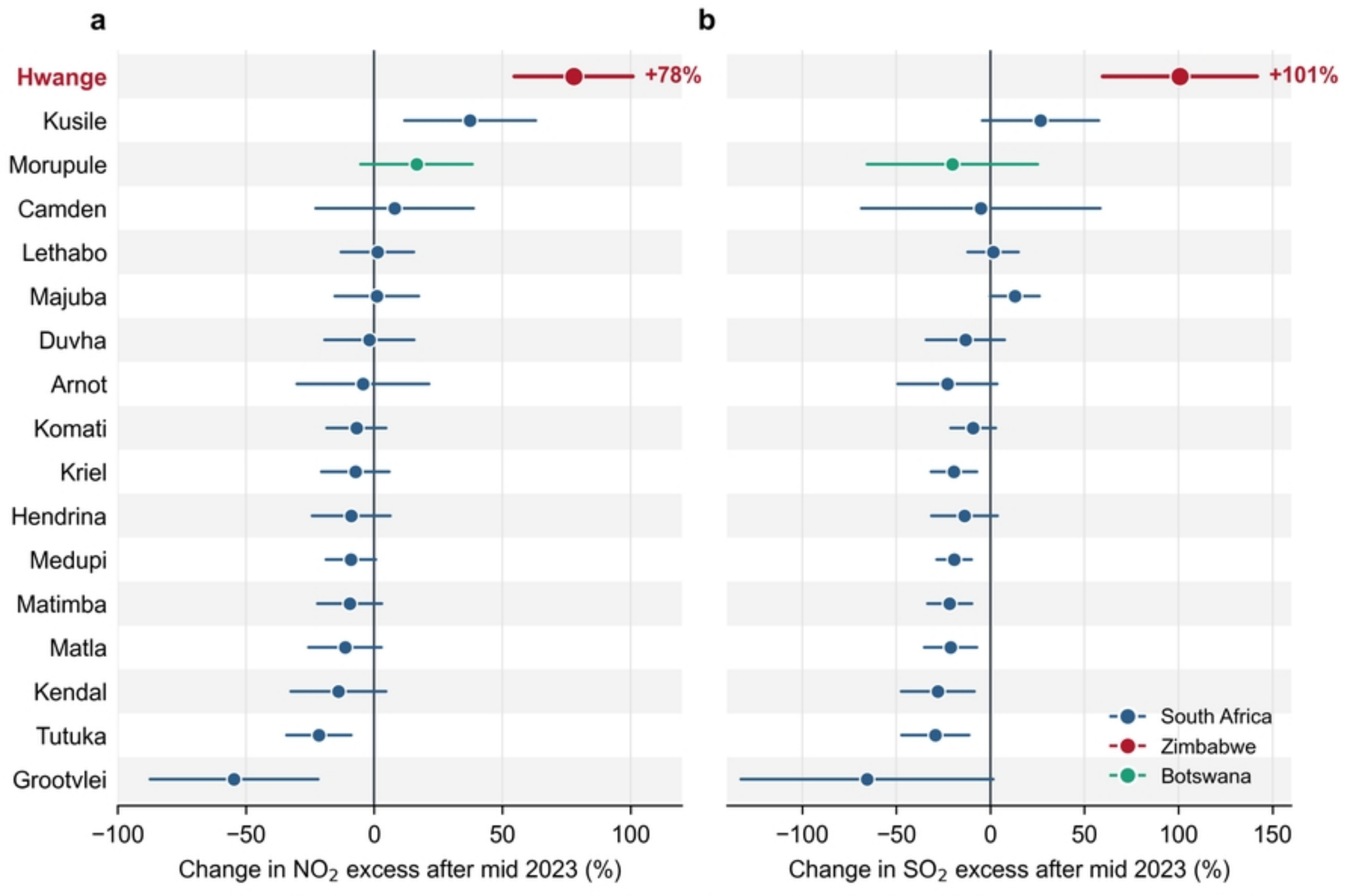


Figure 4



Points: mean change between the same calendar months before (Jul 2018 to Feb 2023) and after (Jul 2023 to Sep 2026); lines: 95% CI.

Figure 5

This manuscript is a preprint and has not been peer reviewed. The copyright holder has made the manuscript available under a Creative Commons Attribution 4.0 International (CC BY) license and consented to have it forwarded to EarthArXiv for public posting.

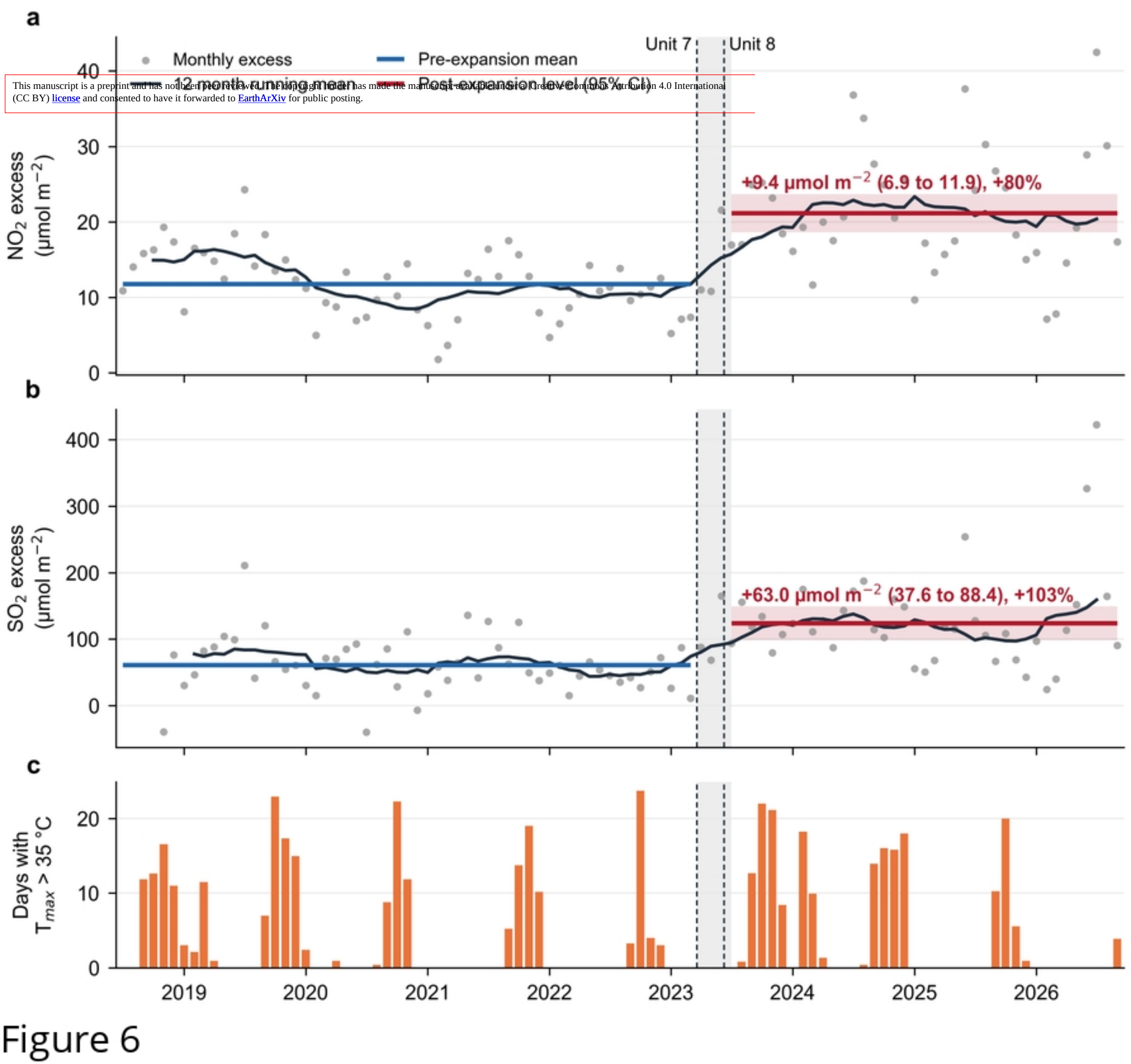


Figure 6

This manuscript is a preprint and has not been peer reviewed. The copyright holder has made the manuscript available under a Creative Commons Attribution 4.0 International (CC BY) license and consented to have it forwarded to EarthArXiv for public posting.

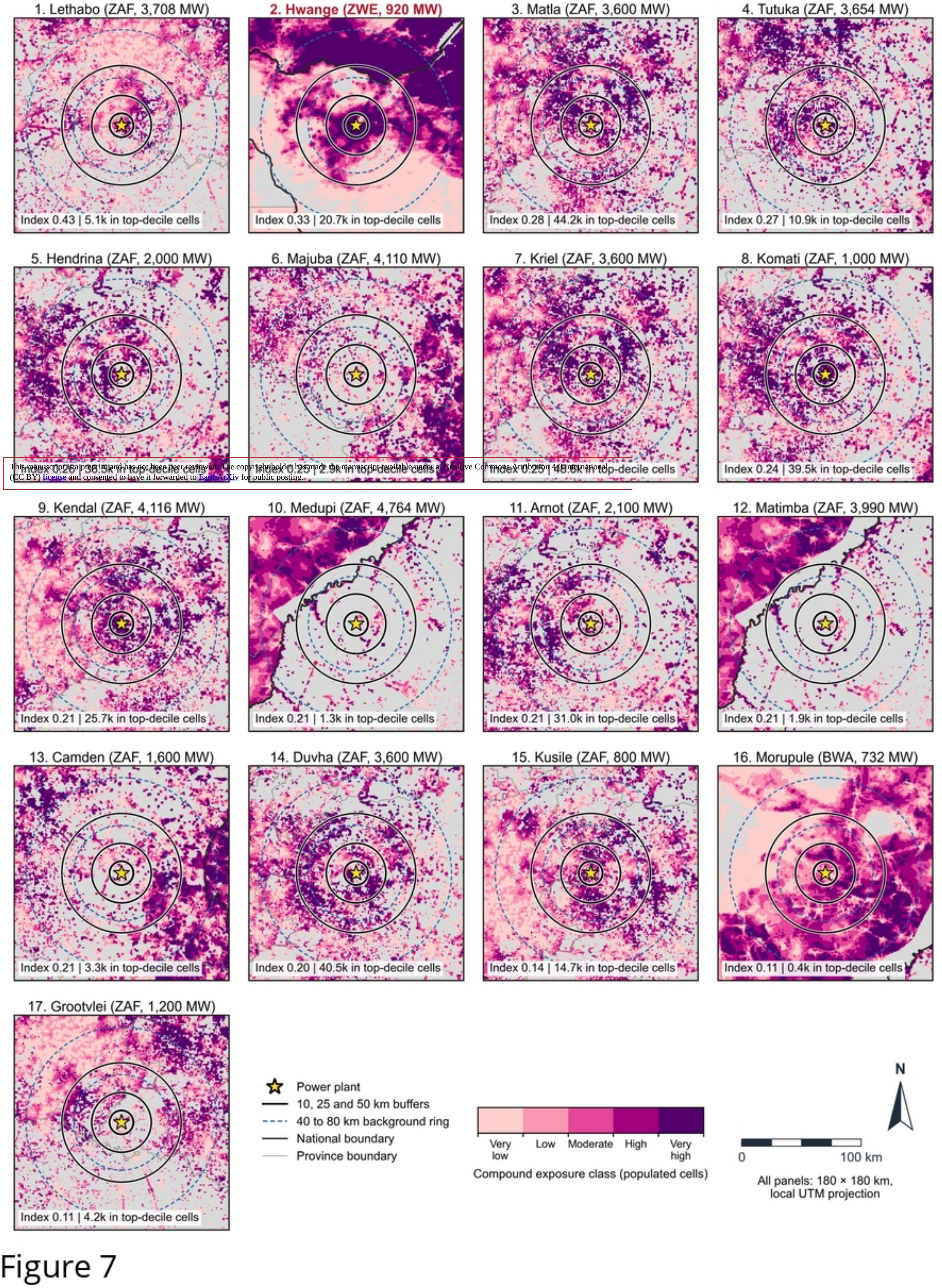


Figure 7

This manuscript is a preprint and has not been peer reviewed. The copyright holder has made the manuscript available under a Creative Commons Attribution 4.0 International (CC BY) license and consented to have it forwarded to EarthArXiv for public posting.

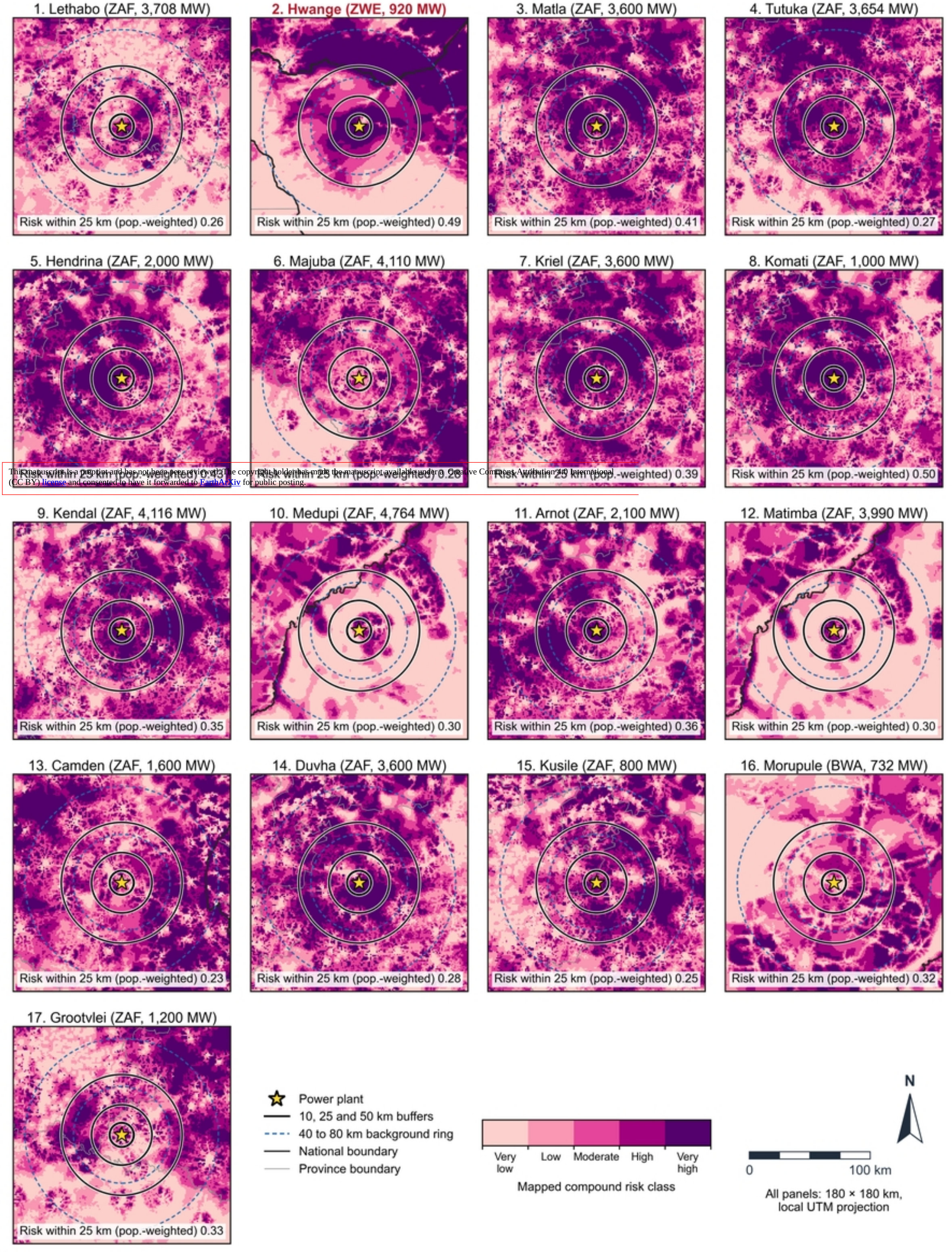


Figure 8